

PROJECTION BASED SEMI-IMPLICIT PARTITIONED REDUCED BASIS METHOD FOR NON-PARAMETRIZED AND PARAMETRIZED FLUID-STRUCTURE INTERACTION PROBLEMS

MONICA NONINO¹, FRANCESCO BALLARIN², GIANLUIGI ROZZA³, YVON MADAY⁴

ABSTRACT. The goal of this manuscript is to present a partitioned Model Order Reduction method that is based on a semi-implicit projection scheme to solve multiphysics problems. We implement a Reduced Order Method based on a Proper Orthogonal Decomposition, with the aim of addressing both time-dependent and time-independent, parametrized Fluid-Structure Interaction problems, where the fluid is incompressible and the structure is thick and two dimensional.

1. INTRODUCTION

Fluid-Structure Interaction (FSI) problems are a wide spread topic in the applied mathematics community, and despite their intrinsic complicated nature (see for example [23, 33]), they are frequently used for simulation purposes, such as, for example, in naval engineering [43], as well as in biomedical applications (as an example of the implementation of FSI in the medical field see [19, 29, 48, 6, 49, 51, 58, 44, 13]) and in aeronautical engineering (see for example [52, 21, 24, 41, 1, 15]). The complex nature of these coupled problems is reflected not only in their theoretical treatment, but also in the way they are solved numerically. From an numerical point of view, there are two approaches that can be adopted in order to address a FSI problem: the first approach consists of a monolithic procedure [8, 47, 5, 46], whereas the second approach consist of a partitioned (segregated), procedure [9, 25].

In a monolithic algorithm the fluid and the solid problem are solved *simultaneously*: this usually results in algorithms that are more stable, which is highly desirable, especially if we wish to use large timesteps in the simulations. The main drawback is given by the fact that they deeply rely on the availability of an *ad hoc software* that can be used to solve both the fluid problem and the solid problem: in this sense, monolithic algorithms are less flexible and more tailored to the particular problem at hand. In the literature there are many examples of works that are based on a monolithic approach: in [29] the author focuses on a monolithic algorithm to address a coupled problem written within the Arbitrary Lagrangian Eulerian (ALE) formalism, where the solid is made of a porous media, and this problem is strictly related to the modelization of the interaction between the blood flow and the arterial walls; another example of FSI problems related to the blood flow-arterial interaction can be found in [59]. In [30] the authors propose different preconditioners, to be used in a Newton-Krylov method for the nonlinear problem arising from solving in a monolithic fashion a coupled problem; another work which focuses on preconditioners for monolithic approaches is the one presented in [20]. We refer the reader interested in a general introduction to monolithic approaches to FSI problems to [53].

As an alternative to monolithic approaches, one can think of adopting a partitioned procedure; indeed, existing simulation tools for fluid dynamics and for structural dynamics are well developed and are used on a daily basis in industrial applications. It is therefore natural to try to combine these computational tools, to address coupled problems: this is exactly the rationale behind a partitioned algorithm. In a partitioned procedure, we solve *separately* the fluid and the solid problem, and

¹ UNIVERSITY OF VIENNA, DEPARTMENT OF MATHEMATICS, VIENNA, AUSTRIA.

² CATHOLIC UNIVERSITY OF THE SACRED HEART, DEPARTMENT OF MATHEMATICS AND PHYSICS, BRESCIA, ITALY.

³ MATHLAB, MATHEMATICS AREA, SISSA, TRIESTE, ITALY.

⁴ SORBONNE UNIVERSITÉ, CNRS, UNIVERSITÉ DE PARIS, LABORATOIRE JACQUES-LOUIS LIONS, PARIS, FRANCE.

then we couple the two physics with some iterative procedure, see for example [32]. Partitioned approaches are very flexible, as they allow to design the procedure in different ways, according to the problem under consideration. In [17], the authors propose a segregated algorithm to solve a FSI problem, where the coupling of the two physics at the fluid–structure interface is taken care of through a constrained optimization problem. In [27, 28] the authors consider the problem of coupling an incompressible fluid with a thin structure; in [27] the authors propose a Robin–Neumann type of coupling at the fluid–structure interface, whereas in [28] the authors propose and explain different couplings techniques at the fluid–structure interface, within an explicit coupling setting. On the contrary, in [26] the authors deal with a problem that has a strong added mass effect (see for example [16]), which is typically the case for the blood in the vessels: in this case, an implicit coupling is the way to control the stability issues due to the added mass effect. Nevertheless, it is clear that a fully implicit treatment of the coupling conditions leads to prohibitive computational costs; for this reason, in [26] the authors propose a semi-implicit coupling technique, which is the approach that will be adopted in this manuscript.

Addressing a coupled problem by means of a partitioned procedure is advantageous in terms of computational efficiency, also from the Reduced Order Model point of view: indeed, in the online phase of the Reduced Basis Method [50, 54, 55, 56, 40, 39], we have to solve, separately, smaller systems. Moreover, with some minor changes such as change of variables and appropriate choices for the couplings, it is possible to further reduce the dimension of the online systems, as we will see in the following.

In this manuscript we design a segregated procedure, combined with a Reduced Order Model based on a Proper Orthogonal Decomposition, and to test and analyze the performance of the obtained algorithm on three test cases. The goal is to extend the work done in [9], moving to the treatment of a two dimensional structure within an Arbitrary Lagrangian Eulerian formalism. The goal is also to extend the work done in [2, 3], adapting the computation and the treatment of the Robin coupling condition, also to the case of a thick, two dimensional structure.

This manuscript is structured as follows: in Section 2 we briefly introduce the Arbitrary Lagrangian Formulation, and we set the notation that will be used throughout the manuscript. In Section 3 we introduce the first test case, namely a time dependent, non parametrized FSI problem that models the interaction of a fluid with a thick, two dimensional, structure; in Section 3.2 we introduce the partitioned procedure at the high order level. In Section 3.3 we derive the partitioned procedure at the reduced order level, and in Section 3.4 we present the numerical results. In Section 4 we consider the same problem of interest, with the addition of a shape parametrization: in Section 4.1 we present the ALE formalism in the presence of a geometrical parametrization of the domain; in Section 4.2 we give the strong formulation of the problem of interest, and in Section 4.3 we describe the algorithm at the high order level. In Section 4.4 we introduce the reduced order model, and then we present some numerical results in Section 4.5. In Section 5 we introduce the last test case, which is the same problem of interest, with a shape parametrization and a physical parametrization: in Section 5.2 we present the offline phase, where we explain the POD technique used in order to handle multiple parameters; in Section 5.3 we present the online phase and in Section 5.4 we show some numerical results. After the conclusions in Section 6, we present an Appendix with some calculations that will be used in this manuscript.

2. CONFIGURATIONS, DEFINITIONS AND NOTATION

In this Section we are going to introduce briefly the Arbitrary Lagrangian Eulerian (ALE) formalism, in order to set the notation that will be used throughout the rest of this manuscript. One of the many difficulties that characterize FSI problems is represented by the fact that the fluid domain in FSI applications is a moving domain; in solid mechanics it is common to deal with moving domains, and the deformation of the domain is usually the unknown of the problem; for fluid dynamics instead one usually considers fixed domains. This different point of view is an intrinsic peculiarity of the FSI problems, and it gives rise to a formalism, very known and widely used in the community, which is called the *Arbitrary Lagrangian Eulerian formulation* [53, 22, 38, 12].

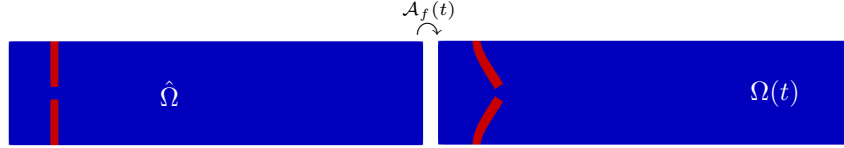


FIGURE 1. Example: domain reference configuration $\hat{\Omega}$ (left) and domain original configuration at time t , $\Omega(t)$ (right). In blue we have the fluid domain, in red the solid domain.

Let $\Omega(t) \subset \mathbb{R}^2$ be the physical domain over which the FSI problem is formulated, with time $t \in [0, T]$: $\Omega(t) = \Omega_f(t) \cup \Omega_s(t)$, where $\Omega_f(t) \subset \mathbb{R}^2$ and $\Omega_s(t) \subset \mathbb{R}^2$ are the fluid and the solid domain at time t , respectively; we assume that the two domains do not overlap, i.e. $\Omega_f(t) \cap \Omega_s(t) = \emptyset$, and finally, the fluid–structure interface $\Gamma_{FSI}(t)$ is defined as $\Gamma_{FSI}(t) := \bar{\Omega}_f(t) \cap \bar{\Omega}_s(t)$. To describe the behaviour of a solid it is common practice to use the so called *Lagrangian formalism*: all the quantities and the conservation laws are formulated on the reference configuration $\hat{\Omega}_s = \Omega_s(t = 0)$. On the contrary, when describing the behaviour of a fluid, the *Eulerian formalism* is used instead: all the quantities and the conservation laws are formulated on the configuration $\Omega_f(t)$ at the current time t . In order to be able to describe both the fluid and the solid, a mixed formulation (the ALE formulation indeed) is used: the underlying idea is that of pulling back the fluid equations to an arbitrary time-independent configuration $\hat{\Omega}_f$: one possible choice for $\hat{\Omega}_f$ is $\hat{\Omega}_f = \Omega_f(t = 0)$, the domain at initial time. In Figure 1 we can see an example of a reference configuration and the configuration of the domain at the current time t . Let us see in the next paragraph how to introduce the ALE formalism; for a more detailed discussion about different approaches to describe coupled systems we refer to [37, 53].

Let $[0, T]$ be a time interval, and let $\hat{\Omega}_f$ be a *reference configuration* for the fluid.

Definition 2.1. *The ALE mapping $\mathcal{A}_f(t)$, for every $t \in [0, T]$ is defined as follows:*

$$\begin{aligned} \mathcal{A}_f(t): \hat{\Omega}_f &\mapsto \Omega_f(t) \\ \hat{\boldsymbol{x}} &\mapsto \boldsymbol{x} = \hat{\boldsymbol{x}} + \hat{\boldsymbol{d}}_f(\hat{\boldsymbol{x}}, t), \end{aligned}$$

where $\hat{\boldsymbol{d}}_f(t): \hat{\Omega}_f \mapsto \hat{\Omega}_f$ is the *mesh displacement*. There are different possibilities for the definition of the mesh displacement: in this manuscript, we decide to define $\hat{\boldsymbol{d}}_f$ as an harmonic extension of the solid displacement $\hat{\boldsymbol{d}}_s$ on the whole fluid domain $\hat{\Omega}_f$:

$$\begin{cases} -\hat{\Delta} \hat{\boldsymbol{d}}_f = 0 & \text{in } \hat{\Omega}_f, \\ \hat{\boldsymbol{d}}_f = \hat{\boldsymbol{d}}_s & \text{on } \hat{\Gamma}_{FSI}, \end{cases}$$

where $\hat{\Gamma}_{FSI}$ is the fluid–structure interface in the reference configuration. A great attention has to be paid to the definition of the mesh displacement, as different choices for $\hat{\boldsymbol{d}}_f$ lead to different degrees of regularity: if we loose regularity due to the mesh displacement, we consequently loose regularity at the FSI interface, which is exactly where the coupling between the two physics takes place. It is beyond the scope of this work to discuss the regularity of different definitions of the mesh displacement; nonetheless we refer the interested reader to Chapter 5.3.5 of [53].

Remark 2.2. $\hat{\boldsymbol{d}}_f$ represents the displacement of the grid points, therefore it is not a quantity with a real physical meaning, but rather a geometrical quantity that describes the deformation of the mesh, according to the deformation of the physical domain. It is also important to underline that $\partial_t \hat{\boldsymbol{d}}_f \neq \hat{\boldsymbol{u}}_f$: in fact, while $\hat{\boldsymbol{u}}_f$ represents the velocity of the fluid, $\partial_t \hat{\boldsymbol{d}}_f$ is again a geometrical quantity, that can be interpreted as the velocity with which the mesh moves.

Let us now define the gradient \boldsymbol{F} of the ALE map and its determinant J , respectively:

$$\boldsymbol{F} := \hat{\nabla} \mathcal{A}_f, \quad J := \det \boldsymbol{F}.$$



FIGURE 2. Physical reference configuration. Blue domain: the reference fluid configuration $\hat{\Omega}_f$. Red leaflets: the reference solid configuration $\hat{\Omega}_s$. The fluid–structure interface $\hat{\Gamma}_{FSI}$ is depicted in green. $\hat{\Gamma}_s^D$: the part of the leaflets that does not move.

With these quantities we are ready to present the strong formulation of the FSI problem of interest, within an ALE formalism.

3. FIRST TEST CASE: TIME DEPENDENT FSI PROBLEM

We present the first FSI problem of interest: a time–dependent, non parametrized, nonlinear multiphysics test case. The goal is to simulate the behaviour of an incompressible fluid interacting with a deformable solid, in the time interval $[0, T]$; Figure 2 shows the physical domain in its reference configuration.

3.1. Strong formulation. The coupled FSI problem, formulated over the original configuration, reads as follows: find $\mathbf{u}_f: \Omega_f(t) \mapsto \mathbb{R}^2$, $p_f: \Omega_f(t) \mapsto \mathbb{R}$ and $\hat{\mathbf{d}}_s: \hat{\Omega}_s \mapsto \mathbb{R}^2$ such that:

$$(1) \quad \begin{cases} \rho_f(\partial_t \mathbf{u}_f + (\mathbf{u}_f \cdot \nabla) \mathbf{u}_f) - \operatorname{div} \sigma_f(\mathbf{u}_f, p_f) = 0 & \text{in } \Omega_f(t) \times (0, T], \\ \operatorname{div} \mathbf{u}_f = 0 & \text{in } \Omega_f(t) \times (0, T], \\ \rho_s \partial_{tt} \hat{\mathbf{d}}_s - \operatorname{div} \hat{\mathbf{P}}(\hat{\mathbf{d}}_s) = 0 & \text{in } \hat{\Omega}_s \times (0, T], \end{cases}$$

with some suitable initial conditions and boundary conditions, and with some coupling conditions that we are going to introduce subsequently. In system (1), the $\hat{\operatorname{div}}$ denotes the fact that the divergence is computed with respect to $\hat{\mathbf{x}}$, the space variable in the reference configuration. ρ_f and ρ_s are the fluid and the solid density, while σ_f is the fluid *Cauchy stress tensor*, and $\hat{\mathbf{P}}$ is the solid *second Piola–Kirchhoff tensor*, defined respectively as:

$$\begin{aligned} \sigma_f(\mathbf{u}_f, p_f) &= \mu_f(\nabla \mathbf{u}_f + \nabla^T \mathbf{u}_f) - p_f \mathbf{I}, \\ \hat{\mathbf{P}}(\hat{\mathbf{d}}_s) &= \lambda_s \operatorname{tr} \varepsilon_s(\hat{\mathbf{d}}_s) \mathbf{I} + 2\mu_s \varepsilon_s(\hat{\mathbf{d}}_s), \\ \varepsilon_s(\hat{\mathbf{d}}_s) &= \frac{1}{2}(\hat{\nabla} \hat{\mathbf{d}}_s + \hat{\nabla}^T \hat{\mathbf{d}}_s), \end{aligned}$$

where μ_f is the fluid viscosity, λ_s and μ_s are the first and second Lamé constant of the solid, respectively (μ_s is also referred to as *shear modulus*), and \mathbf{I} is the 2×2 identity matrix.

With the formalism introduced in Section 2, we are able to perform a pull–back of the fluid equations onto the fluid reference configuration $\hat{\Omega}_f$; the FSI problem on the reference configuration $\hat{\Omega} := \hat{\Omega}_f \cup \hat{\Omega}_s$ now reads: for every $t \in [0, T]$, find the fluid velocity $\hat{\mathbf{u}}_f(t): \hat{\Omega}_f \mapsto \mathbb{R}^2$, the fluid pressure $\hat{p}_f(t): \hat{\Omega}_f \mapsto \mathbb{R}$, the fluid displacement $\hat{\mathbf{d}}_f(t): \hat{\Omega}_f \mapsto \mathbb{R}^2$ and the solid deformation $\hat{\mathbf{d}}_s(t): \hat{\Omega}_s \mapsto \mathbb{R}^2$ such that

$$(2) \quad \begin{cases} \rho_f J(\partial_t \hat{\mathbf{u}}_f + \hat{\nabla} \hat{\mathbf{u}}_f \mathbf{F}^{-1}(\hat{\mathbf{u}}_f - \partial_t \hat{\mathbf{d}}_f)) - \hat{\operatorname{div}}(J \hat{\sigma}_f(\hat{\mathbf{u}}_f, \hat{p}_f) \mathbf{F}^{-T}) = 0 & \text{in } \hat{\Omega}_f \times (0, T], \\ \hat{\operatorname{div}}(J \mathbf{F}^{-1} \hat{\mathbf{u}}_f) = 0 & \text{in } \hat{\Omega}_f \times (0, T], \\ -\hat{\Delta} \hat{\mathbf{d}}_f = 0 & \text{in } \hat{\Omega}_f \times (0, T], \\ \rho_s \partial_{tt} \hat{\mathbf{d}}_s - \operatorname{div} \hat{\mathbf{P}}(\hat{\mathbf{d}}_s) = 0 & \text{in } \hat{\Omega}_s \times (0, T]. \end{cases}$$

The fluid tensor $\hat{\sigma}_f$ is the representation in the reference configuration of the Cauchy stress tensor:

$$\hat{\sigma}_f(\hat{\mathbf{u}}_f, \hat{p}_f) = \mu_f(\hat{\nabla}\hat{\mathbf{u}}_f\mathbf{F}^{-1} + \mathbf{F}^{-T}\hat{\nabla}^T\hat{\mathbf{u}}_f) - \hat{p}_f\mathbf{I},$$

System (2) is completed by some suitable initial conditions, by the boundary conditions

$$\begin{cases} J\hat{\sigma}_f(\hat{\mathbf{u}}_f, \hat{p}_f)\mathbf{F}^{-T}\hat{\mathbf{n}} = -p_{in}(t)\hat{\mathbf{n}} & \text{on } \hat{\Gamma}_{in}, \\ J\hat{\sigma}_f(\hat{\mathbf{u}}_f, \hat{p}_f)\mathbf{F}^{-T}\hat{\mathbf{n}} = 0 & \text{on } \hat{\Gamma}_{out}, \\ \hat{\mathbf{d}}_s = 0 & \text{on } \hat{\Gamma}_s^D, \end{cases}$$

and by the following coupling conditions:

$$(3) \quad \begin{cases} \hat{\mathbf{d}}_f = \hat{\mathbf{d}}_s & \text{on } \hat{\Gamma}_{FSI} \\ \hat{\mathbf{u}}_f = \partial_t\hat{\mathbf{d}}_s & \text{on } \hat{\Gamma}_{FSI}, \\ J\hat{\sigma}_f(\hat{\mathbf{u}}_f, \hat{p}_f)\mathbf{F}^{-T}\hat{\mathbf{n}}_f = -\hat{\mathbf{P}}(\hat{\mathbf{d}}_s)\hat{\mathbf{n}}_s & \text{on } \hat{\Gamma}_{FSI}. \end{cases}$$

In the previous equations the vector $\hat{\mathbf{n}}$ represents the normal vector to the inlet (or outlet) boundary in the reference configuration, whereas $\hat{\mathbf{n}}_f$ is the vector normal to the FSI interface $\hat{\Gamma}_{FSI}$, outgoing the fluid domain, and $\hat{\mathbf{n}}_s$ is the vector normal to the FSI interface $\hat{\Gamma}_{FSI}$, outgoing the solid domain.

Remark 3.1. The gradient and the divergence in equation (2) are computed with respect to the spatial coordinates in the reference configuration, namely $\hat{\mathbf{x}}$. Nevertheless, from now on, since everything will be formulated and computed on the reference configuration, in order to ease the exposition, we will drop the $\hat{\cdot}$ notation.

3.2. Offline computational phase. We are now going to describe the offline phase of the partitioned procedure that we use to solve the FSI problem of this Section. The algorithm is based on a Chorin-Temam projection scheme for the incompressible Navier–Stokes equations [36, 34], and we choose to treat the coupling conditions (3) in a semi-implicit way (see also [9, 4, 26]). We first apply a time stepping procedure to design the algorithm, and then we show the space discretization of the whole procedure.

3.2.1. High fidelity semi-implicit scheme. We present the offline phase of the partitioned procedure: we use an operator splitting approach, based on a Chorin-Temam projection scheme with pressure Poisson formulation. The coupling between fluid and solid problem is imposed through a Robin coupling.

Let ΔT be a timestep: we discretize the time interval $[0, T]$ with an equispaced sampling $\{t_0, \dots, t_{N_T}\}$, where $t_i = i\Delta T$, for $i = 0, \dots, N_T$ and $N_T = \frac{T}{\Delta T}$. We discretize the partial derivative of a function f with a first backward difference: $D_t f^{i+1} = \frac{f^{i+1} - f^i}{\Delta T}$, and $D_{tt} f^{i+1} = D_t(D_t f^{i+1})$, where $f^{i+1} = f(t^{i+1})$. Our partitioned scheme reads as follows: for $i = 0, \dots, N_T$:

Extrapolation of the mesh displacement \mathbf{d}_f : find $\mathbf{d}_f^{i+1}: \Omega_f \mapsto \mathbb{R}^2$ such that:

$$(4) \quad \begin{cases} -\Delta \mathbf{d}_f^{i+1} = 0 & \text{in } \Omega_f, \\ \mathbf{d}_f^{i+1} = \mathbf{d}_s^i & \text{on } \Gamma_{FSI}. \end{cases}$$

Fluid explicit step: find $\mathbf{u}_f^{i+1}: \Omega_f \mapsto \mathbb{R}^2$ such that:

$$(5) \quad \begin{cases} J\rho_f \left(D_t \mathbf{u}_f^{i+1} + \nabla \mathbf{u}_f^{i+1} \mathbf{F}^{-1} (\mathbf{u}_f^{i+1} - D_t \mathbf{d}_f^{i+1}) \right) - \mu_f \operatorname{div}(J\varepsilon(\mathbf{u}_f^{i+1})\mathbf{F}^{-T}) + \\ + J\mathbf{F}^{-T}\nabla p_f^i = 0 & \text{in } \Omega_f, \\ \mathbf{u}_f^{i+1} = D_t \mathbf{d}_f^{i+1} & \text{on } \Gamma_{FSI}, \end{cases}$$

with $\varepsilon(\mathbf{u}_f^{i+1}) := \mu_f(\nabla \mathbf{u}_f \mathbf{F}^{-1} + \mathbf{F}^{-T}\nabla^T \mathbf{u}_f)$.

Implicit step:

- **fluid projection substep (pressure Poisson formulation):** find $p_f^{i+1}: \Omega_f \mapsto \mathbb{R}^2$ such that:

$$(6) \quad \begin{cases} -\operatorname{div}(J\mathbf{F}^{-1}\mathbf{F}^{-T}\nabla p_f^{i+1}) = -\frac{\rho_f}{\Delta t}\operatorname{div}(J\mathbf{F}^{-1}\mathbf{u}_f^{i+1}) & \text{in } \Omega_f, \\ -\mathbf{F}^{-T}\nabla p_f^{i+1} \cdot J\mathbf{F}^{-T}\mathbf{n}_f = \rho_f D_{tt}\mathbf{d}_s^{i+1} \cdot J\mathbf{F}^{-T}\mathbf{n}_f & \text{on } \Gamma_{FSI}, \end{cases}$$

subject to the boundary conditions:

$$(7) \quad \begin{cases} p_f^{i+1} = p_{in}(t^{i+1}) & \text{on } \Gamma_{in} \\ p_f^{i+1} = 0 & \text{on } \Gamma_{out}, \end{cases}$$

- **structure projection substep:** find $\mathbf{d}_s^{i+1}: \Omega_s \mapsto \mathbb{R}^2$ such that:

$$(8) \quad \begin{cases} \rho_s D_{tt}\mathbf{d}_s^{i+1} - \operatorname{div}\mathbf{P}(\mathbf{d}_s^{i+1}) = 0 & \text{in } \Omega_s, \\ J\sigma_f(\mathbf{u}_f^{i+1}, p_f^{i+1})\mathbf{F}^{-T}\mathbf{n}_f = -\mathbf{P}(\mathbf{d}_s^{i+1})\mathbf{n}_s & \text{on } \Gamma_{FSI}. \end{cases}$$

subject to the boundary condition $\mathbf{d}_s^{i+1} = 0$ on Γ_s^D .

Remark 3.2. In the implicit step (6) we have chosen a pressure Poisson formulation; an alternative is to use a Darcy formulation, which is defined as follows: find p_f^{i+1} and $\tilde{\mathbf{u}}_f^{i+1}$ such that:

$$\begin{cases} \rho_f J \frac{\tilde{\mathbf{u}}_f^{i+1} - \mathbf{u}_f^{i+1}}{\Delta T} + J\mathbf{F}^{-T}\nabla p_f^{i+1} = 0 & \text{in } \Omega_f, \\ \operatorname{div}(J\mathbf{F}^{-1}\tilde{\mathbf{u}}_f^{i+1}) = 0 & \text{in } \Omega_f. \end{cases}$$

Throughout this manuscript we choose to employ a Poisson formulation, for the sake of a more efficient reduced order model, since the Darcy formulation requires the introduction of an additional unknown $\tilde{\mathbf{u}}_f$, which translates in a larger system, comprised of both velocity and pressure, at the implicit step.

In order to enhance the stability of the projection scheme, we employ a Robin–Neumann coupling, as proposed in [2, 9]; for other references on this kind of coupling, we refer to [3, 28]. We thus replace condition (6)₂ with the following:

$$(9) \quad \alpha_{ROB} p^{i+1} + \mathbf{F}^{-T}\nabla p^{i+1} \cdot J\mathbf{F}^{-T}\mathbf{n}_f = \alpha_{ROB} p^{i+1,*} - \rho_f D_{tt}\mathbf{d}_s^{i+1,*} \cdot J\mathbf{F}^{-T}\mathbf{n}_f.$$

In equation (9), $p^{i+1,*}$ and $\mathbf{d}_s^{i+1,*}$ are suitable extrapolations of the fluid pressure and the solid displacement, respectively; we show in the next paragraph which kind of extrapolation we use. The constant α_{ROB} is defined as $\alpha_{ROB} = \frac{\rho_f}{z_p \Delta T}$ where z_p is called the *solid impedance*:

$$\begin{aligned} z_p &= \rho_s c_p, \\ c_p &= \sqrt{\frac{\lambda_s + 2\mu_s}{\rho_s}}. \end{aligned}$$

In Appendix A we show more in detail how to compute the coupling condition (9), starting from the idea proposed in [10].

3.2.2. Space discretization of the semi-implicit procedure. We now present the space discretized version of the algorithm introduced. We define the following function spaces for the fluid:

$$V(\Omega_f) := [H^1(\Omega_f)]^2, \quad E^f(\Omega_f) := [H^1(\Omega_f)]^2, \quad Q(\Omega_f) := L^2(\Omega_f),$$

endowed with the H^1 norm ($V(\Omega_f)$ and $E^f(\Omega_f)$) and the L^2 norm respectively, and the function space for the solid: $E^s(\Omega_s) = [H^1(\Omega_s)]^2$, endowed with the H^1 norm. We discretize in space the FSI problem, using second order Lagrange Finite Elements for the fluid velocity, the fluid displacement and the solid displacement, resulting in the discrete spaces $V_h \subset V$, $E_h^f \subset E^f$ and $E_h^s \subset E^s$, while for the fluid pressure we use first order Lagrange Finite Elements, resulting in the discrete space $Q_h \subset Q$. The non-homogeneous boundary condition (7)₁ can be easily treated by introducing, at timestep t^{i+1} , a lifting function ℓ^{i+1} such that $\ell^{i+1} = p_{in}(t^{i+1})$ on Γ_{in} and $\ell^{i+1} = 0$ on Γ_{out} ; we

refer, for example, to [7, 46] for more details concerning the use of a lifting function within model order reduction. By introducing the homogenized pressure $p_f^{0,i+1} := p_f^{0,i+1} - \ell^{i+1}$, we can conclude now that $p_f^{0,i+1} \in Q_h^0$, where $Q_h^0 = \{q_h \in Q_h : q_h = 0 \text{ on } \Gamma_{in} \cup \Gamma_{out}\}$. The discretized version of the semi-implicit procedure reads as follows: for $i = 0, \dots, N_T$,

Extrapolation of the mesh displacement: find $\mathbf{d}_{f,h}^{i+1} \in E_h^f$ such that $\forall \mathbf{e}_{f,h} \in E_h^f$:

$$(10) \quad \begin{cases} \int_{\Omega_f} \mathbf{d}_{f,h}^{i+1} \cdot \mathbf{e}_{f,h} \, dx = 0, \\ \mathbf{d}_{f,h}^{i+1} = \mathbf{d}_{s,h}^i \quad \text{on } \Gamma_{FSI}. \end{cases}$$

Fluid explicit step: find $\mathbf{u}_{f,h}^{i+1} \in V_h$ such that $\forall \mathbf{v}_h \in V_h$:

$$(11) \quad \begin{cases} \rho_f \int_{\Omega_f} J D_t \mathbf{u}_{f,h}^{i+1} \cdot \mathbf{v}_h \, dx + \rho_f \int_{\Omega_f} J (\nabla \mathbf{u}_{f,h}^{i+1} \mathbf{F}^{-1} (\mathbf{u}_{f,h}^{i+1} - D_t \mathbf{d}_{f,h}^{i+1})) \cdot \mathbf{v}_h \, dx \\ + \mu_f \int_{\Omega_f} J \varepsilon (\mathbf{u}_{f,h}^{i+1}) \mathbf{F}^{-T} : \nabla \mathbf{v}_h \, dx + \int_{\Omega_f} J \mathbf{F}^{-T} \nabla p_{f,h}^i \cdot \mathbf{v}_h \, dx = 0 \\ \mathbf{u}_{f,h}^{i+1} = D_t \mathbf{d}_{f,h}^{i+1} \quad \text{on } \Gamma_{FSI}, \end{cases}$$

Implicit step: for any $j = 0, \dots$ until convergence:

- (1) **fluid projection substep (pressure Poisson formulation):** find $p_{f,h}^{0,i+1,j+1} \in Q_h^0$ such that $\forall q_h \in Q_h^0$:

$$\begin{aligned} & \alpha_{ROB} \int_{\Gamma_{FSI}} p_{f,h}^{0,i+1,j+1} q_h \, ds + \int_{\Omega_f} J \mathbf{F}^{-T} \nabla p_{f,h}^{0,i+1,j+1} \cdot \mathbf{F}^{-T} \nabla q_h \, dx = \\ & - \frac{\rho_f}{\Delta T} \int_{\Omega_f} \operatorname{div} (J \mathbf{F}^{-1} \mathbf{u}_{f,h}^{i+1}) q_h \, dx - \rho_f \int_{\Gamma_{FSI}} D_{tt} \mathbf{d}_{s,h}^{i+1,j} \cdot J \mathbf{F}^{-T} \mathbf{n}_f q_h \, ds \\ & + \alpha_{ROB} \int_{\Gamma_{FSI}} p_{f,h}^{i+1,j} q_h \, ds - \alpha_{ROB} \int_{\Gamma_{FSI}} \ell^{i+1} q_h \, ds - \int_{\Omega_f} J \mathbf{F}^{-T} \nabla \ell^{i+1} \cdot \mathbf{F}^{-T} \nabla q_h \, dx, \end{aligned}$$

- (2) **structure projection substep:** find $\mathbf{d}_{s,h}^{i+1,j+1} \in E_h^s$ such that $\forall \mathbf{e}_{s,h} \in E_h^s$:

$$\begin{aligned} & \rho_s \int_{\Omega_s} D_{tt} \mathbf{d}_{s,h}^{i+1,j+1} \cdot \mathbf{e}_{s,h} \, dx + \int_{\Omega_s} \mathbf{P}(\mathbf{d}_{s,h}^{i+1,j+1}) : \nabla \mathbf{e}_{s,h} \, dx = \\ & - \int_{\Gamma_{FSI}} J \sigma_f (\mathbf{u}_{f,h}^{i+1}, p_{f,h}^{i+1,j+1}) \mathbf{F}^{-T} \mathbf{n}_f \cdot \mathbf{e}_{s,h} \, dx, \end{aligned}$$

subject to the boundary condition $\mathbf{d}_{s,h}^{i+1,j+1} = 0$ on Γ_D^s .

We iterate between the two implicit substeps, until a convergence criteria is satisfied; we choose as stopping criteria a relative error on the increments of the pressure and the solid displacement, namely:

$$\max \left(\frac{\|p_{f,h}^{i+1,j+1} - p_{f,h}^{i+1,j}\|_{Q_h}}{\|p_{f,h}^{i+1,j+1}\|_{Q_h}}; \frac{\|\mathbf{d}_{s,h}^{i+1,j+1} - \mathbf{d}_{s,h}^{i+1,j}\|_{E_h^s}}{\|\mathbf{d}_{s,h}^{i+1,j+1}\|_{E_h^s}} \right) < \varepsilon,$$

where ε is a fixed tolerance.

In the pressure Poisson formulation, to impose the Robin coupling condition, we have chosen the pressure at the previous implicit iteration, namely $p_f^{i+1,j}$, as an extrapolation for the fluid pressure, and the same goes for the extrapolation of the structure displacement.

3.2.3. POD and reduced basis generation. For the generation of the reduced basis for the fluid velocity \mathbf{u}_f and the fluid displacement \mathbf{d}_f we pursue here the idea that was first proposed in [9]. For the homogenized fluid pressure p_f^0 and for the solid displacement \mathbf{d}_s we employ a standard POD.

Change of variable for the fluid velocity. The main idea here is to introduce a change of variable in the fluid problem, in order to transform condition (30)₂ into a homogeneous boundary condition. The motivation of this choice is that, to impose condition (30)₂, we could use a Lagrange multiplier λ , but the introduction of a further variable leads to an increased dimension of the system to be solved in the online phase. Therefore, in order to avoid this and in order to design a more efficient reduced method, we choose to transform the non-homogeneous coupling condition into a homogeneous one. In order to do this, we define a new variable $\mathbf{z}_{f,h}^{i+1}$:

$$\mathbf{z}_{f,h}^{i+1} := \mathbf{u}_{f,h}^{i+1} - D_t \mathbf{d}_{f,h}^{i+1}.$$

With this change of variable, equation (30)₂ is equivalent to the homogeneous boundary condition for the new variable:

$$\mathbf{z}_{f,h}^{i+1} = 0 \quad \text{on } \Gamma_{FSI},$$

for which no imposition by means of Lagrange multiplier is needed. Therefore, during the offline phase of the algorithm, at every iteration $i+1$, after we have computed the velocity $\mathbf{u}_{f,h}^{i+1}$, we compute the change of variable $\mathbf{z}_{f,h}^{i+1}$. We then consider the following snapshots matrix:

$$\mathcal{S}_z = [\mathbf{z}_{f,h}^1, \dots, \mathbf{z}_{f,h}^{N_T}] \in \mathbb{R}^{\mathcal{N}_u^h \times N_T},$$

where $\mathcal{N}_u^h = \dim V_h$. We then apply a POD to the snapshots matrix \mathcal{S}_z and we retain the first N_z POD modes $\Phi_z^1, \dots, \Phi_z^{N_z}$. We therefore have the reduced space:

$$V^N := \text{span}\{\Phi_z^k\}_{k=1}^{N_z},$$

and now it is clear that, since every Φ_z^k satisfies the condition $\Phi_z^k = 0$ on Γ_{FSI} , then also every element of V^N will satisfy the same condition.

Harmonic extension of the fluid displacement. In order to generate the reduced basis for the fluid displacement \mathbf{d}_f , we pursue again the idea presented in [9]. Therefore, we start by generating the snapshots matrix related to the solid displacement:

$$\mathcal{S}_{d_s} = [\mathbf{d}_{s,h}^1, \dots, \mathbf{d}_{s,h}^{N_T}] \in \mathbb{R}^{\mathcal{N}_{d_s}^h \times N_T},$$

where $\mathcal{N}_{d_s}^h = \dim E_h^s$. We then apply a POD to the snapshots matrix and retain the first N_d POD modes $\Phi_{d_s}^1, \dots, \Phi_{d_s}^{N_d}$, thus defining the reduced space for the solid problem:

$$E_N^s := \text{span}\{\Phi_{d_s}^k\}_{k=1}^{N_d}.$$

We then employ an harmonic extension of each one of the reduced basis $\Phi_{d_s}^k$ to the fluid domain, thus obtaining the functions $\Phi_{d_f}^k$ such that:

$$\begin{cases} -\Delta \Phi_{d_f}^k = 0 & \text{in } \Omega_f, \\ \Phi_{d_f}^k = \Phi_{d_s}^k & \text{on } \Gamma_{FSI}. \end{cases}$$

We can then define the reduced space for the fluid displacement:

$$E_N^f := \text{span}\{\Phi_{d_f}^k\}_{k=1}^{N_d}.$$

The reason for for this choice, instead of employing a standard POD on the set of snapshots of \mathbf{d}_f , is given by the fact that we can avoid the introduction of another Lagrange multiplier to impose the non-homogeneous boundary condition (29)₂. With our method, we avoid to solve the reduced system related to (29): indeed, instead of solving an harmonic extension problem at every timestep in the online phase, we solve *once and for all* N_d harmonic extension problems in the expensive offline phase. Then, during the online phase, the reduced fluid displacement will be computed just as a linear combination of the basis $\Phi_{d_f}^i$, with coefficients that are the coefficients of the reduced solid displacement at the previous timestep. We will see in the next Section the final formulation of the online phase of the algorithm.

3.3. Online computational phase. We are now ready to present the online formulation of the partitioned procedure. For every $i = 0, \dots, N_T$, we introduce the reduced functions $\mathbf{z}_{f,N}^{i+1}$, $p_{f,N}^{0,i+1}$, $\mathbf{d}_{s,N}^{i+1}$ of the form:

$$(12) \quad \mathbf{z}_{f,N}^{i+1} = \sum_{k=1}^{N_z} \underline{\mathbf{z}}_k^{i+1} \Phi_{\mathbf{z}_f}^k,$$

$$(13) \quad p_{f,N}^{0,i+1} = \sum_{k=1}^{N_p} \underline{p}_k^{0,i+1} \Phi_p^k,$$

$$(14) \quad \mathbf{d}_{s,N}^{i+1} = \sum_{k=1}^{N_d} \underline{\mathbf{d}}_k^{i+1} \Phi_{\mathbf{d}_s}^k.$$

Then the online phase of the partitioned procedure reads as follows:

Mesh displacement: let $\mathbf{d}_{f,N}^{i+1}$ be defined by the reduced solid displacement at the previous timestep:

$$(15) \quad \mathbf{d}_{f,N}^{i+1} = \sum_{k=1}^{N_d} \underline{\mathbf{d}}_k^i \Phi_{\mathbf{d}_f}^k;$$

Fluid explicit step (with change of variable): find $\mathbf{z}_{f,N}^{i+1} \in V_N$ such that $\forall \mathbf{v}_N \in V_N$:

$$\begin{aligned} & \rho_f \int_{\Omega_f} J \left(\frac{\mathbf{z}_{f,N}^{i+1} - \mathbf{u}_{f,N}^i}{\Delta T} \right) \cdot \mathbf{v}_N \, dx + \rho_f \int_{\Omega_f} J (\nabla (\mathbf{z}_{f,N}^{i+1} + D_t \mathbf{d}_{f,N}^{i+1}) \mathbf{F}^{-1} \mathbf{z}_{f,N}^{i+1}) \cdot \mathbf{v}_N \, dx \\ & + \mu_f \int_{\Omega_f} J \varepsilon (\mathbf{z}_{f,N}^{i+1}) \mathbf{F}^{-T} : \nabla \mathbf{v}_N \, dx + \int_{\Omega_f} J \mathbf{F}^{-T} \nabla p_{f,N}^i \cdot \mathbf{v}_h \, dx = \\ & - \rho_f \int_{\Omega_f} J \left(\frac{D_t \mathbf{d}_{f,N}^{i+1}}{\Delta T} \right) \cdot \mathbf{v}_N \, dx - \mu_f \int_{\Omega_f} J \varepsilon (D_t \mathbf{d}_{f,N}^{i+1}) \mathbf{F}^{-T} : \nabla \mathbf{v}_N \, dx, \end{aligned}$$

we then restore the reduced fluid velocity: $\mathbf{u}_{f,N}^{i+1} = \mathbf{z}_{f,N}^{i+1} + D_t \mathbf{d}_{f,N}^{i+1}$.

Implicit step: for any $j = 0, \dots$ until convergence:

(1) **fluid projection substep:** find $p_{f,N}^{0,i+1,j+1} \in Q_N^0$ such that $\forall q_N \in Q_N^0$:

$$\begin{aligned} & \alpha_{ROB} \int_{\Gamma_{FSI}} p_{f,N}^{0,i+1,j+1} q_N \, ds + \int_{\Omega_f} J \mathbf{F}^{-T} \nabla p_{f,N}^{0,i+1,j+1} \cdot \mathbf{F}^{-T} \nabla q_N \, dx = \\ & - \frac{\rho_f}{\Delta T} \int_{\Omega_f} \operatorname{div} (J \mathbf{F}^{-1} \mathbf{u}_{f,N}^{i+1}) q_N \, dx - \rho_f \int_{\Gamma_{FSI}} (D_{tt} \mathbf{d}_{s,N}^{i+1,j}) \cdot J \mathbf{F}^{-T} \mathbf{n}_f q_N \, ds \\ & + \alpha_{ROB} \int_{\Gamma_{FSI}} p_{f,N}^{i+1,j} q_N \, ds - \alpha_{ROB} \int_{\Gamma_{FSI}} \ell^{i+1} q_N \, ds \\ & - \int_{\Omega_f} J \mathbf{F}^{-T} \nabla \ell^{i+1} \cdot \mathbf{F}^{-T} \nabla q_N \, dx \end{aligned}$$

we then recover the reduced fluid pressure $p_{f,N}^{i+1,j+1} = p_{f,N}^{0,i+1,j+1} + \ell^{i+1}$.

(2) **structure projection substep:** find $\mathbf{d}_{s,N}^{i+1,j+1} \in E_N^s$ such that $\forall \mathbf{e}_s \in E_N^s$:

$$\begin{aligned} & \rho_s \int_{\Omega_s} D_{tt} \mathbf{d}_{s,N}^{i+1,j+1} \cdot \mathbf{e}_N \, dx + \int_{\Omega_s} \mathbf{P}(\mathbf{d}_{s,N}^{i+1,j+1}) : \nabla \mathbf{e}_N \, dx = \\ & - \int_{\Omega_s} J \sigma_f (\mathbf{u}_{f,N}^{i+1}, p_{f,N}^{i+1,j+1}) \mathbf{F}^{-T} \mathbf{n}_f \cdot \mathbf{e}_N \, dx. \end{aligned}$$

TABLE 1. Values for the implementation of the offline phase.

Physical constants	Value
ρ_f	1 g/cm ³
μ_f	0.035 Poise
ρ_s	1.1 g/cm ³
μ_s	100000
λ_s	8000
Discretization details	Value
FE displacement order	2
FE velocity order	2
FE pressure order	1

3.4. Numerical results. We now present some numerical results obtained with the semi-implicit scheme. The reference physical configuration of the problem of interest is the one represented in Figure 2: we therefore have two leaflets, made of some elastic material, that bend under the influence of a fluid flow; the fluid domain is 2.5 cm high and 10 cm long; the leaflets are situated 1 cm downstream the inlet boundary, they are 0.2 cm thick and 1.1 cm long. For our simulation we used a timestep $\Delta T = 10^{-4}$, and a final time $T = 0.2$ s, for a total of $N_T = 2000$ iterations.

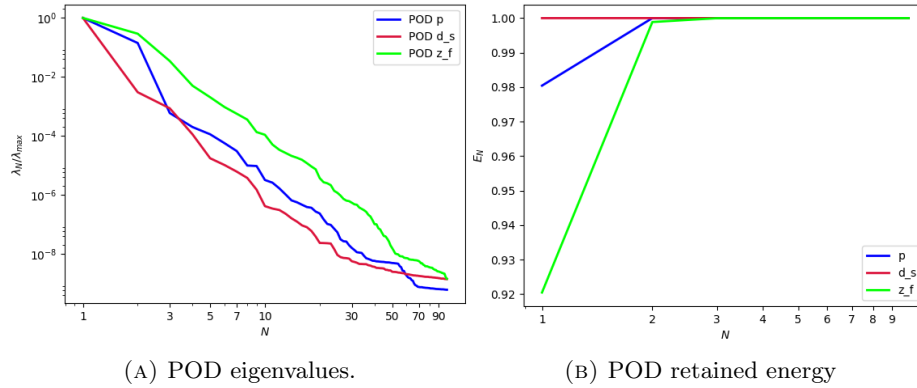
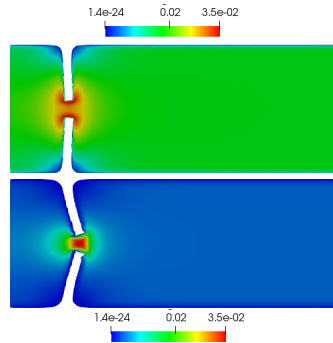


FIGURE 3. Results of the POD for the non parametric problem.

FIGURE 4. Reduced velocity $\mathbf{u}_{f,N}$ at timestep $t = 0.1$ s (top) and at timestep $t = 0.2$ s (bottom). The velocity has been obtained with $N_z = 20$ reduced basis.

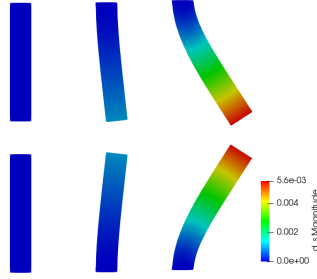


FIGURE 5. Reduced solid displacement $\mathbf{d}_{s,N}$ at timestep $t = 0.02s$ (left), $t = 0.1s$ (center) and at timestep $t = 0.2s$ (right). The displacement has been obtained with $N_d = 20$ reduced basis. The displacement has been magnified for visualization purposes.

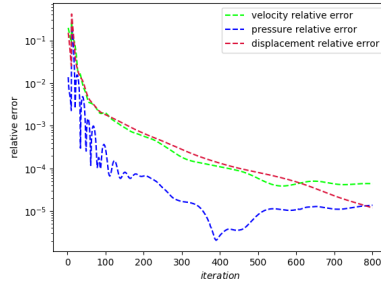


FIGURE 6. Error analysis: relative error behaviour, as a function of time.

The values of the physical constants used in the simulation are reported in Table 1. A pressure impulse $p_{in}(t)$ is applied at the inlet boundary, and after some time this impulse becomes constant:

$$p_{in}(t) = \begin{cases} 5 - 5\cos\left(\frac{2\pi t}{T_{in}}\right) & \text{for } t \leq 0.1s, \\ 5 & \text{for } t > 0.1s, \end{cases}$$

where $T_{in} = 0.4s$. We fix a tolerance of $\varepsilon = 10^{-6}$ as a stopping criterion for the subiterations between the pressure Poisson problem and the solid problem.

Since we do not consider the top and the bottom walls of the fluid domain to be deformable, we impose a homogeneous boundary condition for the fluid velocity on these walls.

Figure 3a shows the rate of decay of the first 100 eigenvalues associated with three unknowns of the problem, namely the change of variable for the fluid velocity \mathbf{z}_f , the pressure p_f and the solid displacement \mathbf{d}_s . It can be noticed that the rate of decay of the eigenvalues for the pressure and for the fluid change of variable is slower than the rate of decay of the eigenvalues of the solid displacement. Moreover, in Figure 3b we can notice that the first mode of the solid displacement retains 2% more energy compared to the first mode of the pressure, and 8% more energy with respect to the first mode of \mathbf{z}_f , which is the one that retains less energy. Figures 4 and 5 show two representative reduced order solutions: the fluid velocity and the solid displacement, respectively; as we can see from Figure 5, the reduced order model shows a good capability also in reproducing very small deformations. Figure 6 shows that, with $N_z = N_p = N_d = 20$ basis functions for each component of the solution, we have a good approximation error behaviour over time.

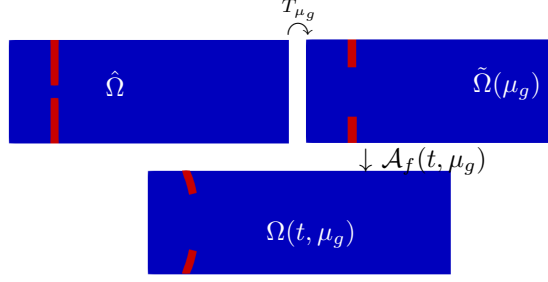


FIGURE 7. Domains: reference configuration $\hat{\Omega}$ (top left), parametrized reference configuration $\tilde{\Omega}(\mu_g)$ (top right), and original configuration $\Omega(t; \mu_g)$ (bottom).

4. SECOND TEST CASE: SHAPE PARAMETRIZATION OF THE LEAFLETS

In this Section we are going to present a test case that is similar to the one previously introduced, the difference being now the presence of a geometrical parameter μ_g , that represents the length of the leaflets.

4.1. ALE formulation in the presence of shape parametrization. Let us denote by $\Omega(t; \mu_g) := \Omega_f(t; \mu_g) \cup \Omega_s(t; \mu_g)$ the current physical domain: we now have a time dependence, and a parameter dependence. We introduce the time-independent *intermediate configuration* $\tilde{\Omega}(\mu_g) := \tilde{\Omega}_f(\mu_g) \cup \tilde{\Omega}_s(\mu_g)$, where we are considering the reference configuration of both physics, still taking into account the parameter dependence. Finally, we have the time-independent, parameter-independent *reference configuration* $\hat{\Omega} := \hat{\Omega}_f \cup \hat{\Omega}_s$.

We call T the shape parametrization map; for every $\mu_g \in \mathcal{P} \subset \mathbb{R}$, where $\mathcal{P} = [\mu_g^{min}, \mu_g^{max}]$ is the domain of the geometrical parameter, we have a map T_{μ_g} defined as follows:

$$\begin{aligned} T_{\mu_g} : \hat{\Omega} &\mapsto \tilde{\Omega}(\mu_g) \\ \hat{x} &\mapsto \tilde{x} = T_{\mu_g}(\hat{x}). \end{aligned}$$

We then have the ALE map $\mathcal{A}_f(t; \mu_g)$, already introduced in Section 2, which is now a map from the current parametrized fluid configuration $\hat{\Omega}_f(t; \mu_g)$ and the intermediate fluid configuration $\tilde{\Omega}_f(\mu_g)$:

$$\begin{aligned} \mathcal{A}_f(t; \mu_g) : \tilde{\Omega}_f(\mu_g) &\mapsto \hat{\Omega}_f(t; \mu_g) \\ \tilde{x} &\mapsto \hat{x} = \tilde{x} + \tilde{\mathbf{d}}_f(\tilde{x}; t, \mu_g), \end{aligned}$$

where $\tilde{\mathbf{d}}_f$ is the mesh displacement already defined in Section 2.

Let us define the gradients and the determinants of the deformation maps:

$$(16) \quad \begin{aligned} \mathbf{G}(\hat{x}; \mu_g) &= \hat{\nabla} T_{\mu_g}(\hat{x}), & K(\hat{x}; \mu_g) &= \det \mathbf{G}(\hat{x}; \mu_g), \\ \tilde{\mathbf{F}}(\tilde{x}; \mu_g) &= \tilde{\text{Id}} + \tilde{\nabla} \tilde{\mathbf{d}}_f, & \tilde{J}(\tilde{x}; \mu_g) &= \det \tilde{\mathbf{F}}. \end{aligned}$$

We can pull-back the gradient $\tilde{\mathbf{F}}(\tilde{x}; \mu_g)$ to the reference domain $\hat{\Omega}_f$, and we obtain $\mathbf{F}(\hat{x}; \mu_g) = \text{Id} + \hat{\nabla} \hat{\mathbf{d}}_f \mathbf{G}^{-1}(\hat{x}, \mu_g)$. With this notation, we can conclude that the gradient of the deformation map from the reference configuration to the current configuration is given by $\mathbf{F}(\hat{x}, \mu_g) \mathbf{G}(\hat{x}, \mu_g)$; let us denote by $\tilde{\mathbf{F}}_{\mu_g}$, \mathbf{F}_{μ_g} and \mathbf{G}_{μ_g} the gradients $\tilde{\mathbf{F}}(\tilde{x}, \mu_g)$, $\mathbf{F}(\hat{x}, \mu_g)$ and $\mathbf{G}(\hat{x}, \mu_g)$ respectively, and by J_{μ_g} and K_{μ_g} the determinants of \mathbf{F}_{μ_g} and \mathbf{G}_{μ_g} . We are now ready to state the strong form of the problem of interest.

4.2. Strong formulation. The strong form of the parametrized FSI problem reads as follows: for every $t \in [0, T]$ and for every $\mu_g \in \mathcal{P}$, find the fluid velocity $\mathbf{u}_f(t; \mu_g) : \Omega_f(t; \mu_g) \mapsto \mathbb{R}^2$, the fluid pressure $p_f(t; \mu_g) : \Omega_f(t; \mu_g) \mapsto \mathbb{R}$, the mesh displacement $\tilde{\mathbf{d}}_f(t; \mu_g) : \tilde{\Omega}_f(\mu_g) \mapsto \mathbb{R}^2$ and the solid

displacement $\tilde{\mathbf{d}}_s(t; \mu_g) : \tilde{\Omega}_s(\mu_g) \mapsto \mathbb{R}^2$ such that:

$$\begin{cases} -\tilde{\Delta} \tilde{\mathbf{d}}_f = 0 & \text{in } \tilde{\Omega}_f(\mu_g) \times [0, T], \\ \tilde{\mathbf{d}}_f = \tilde{\mathbf{d}}_s & \text{on } \tilde{\Gamma}_{FSI} \times [0, T], \end{cases}$$

and

$$\begin{cases} \rho_f \partial_t \mathbf{u}_f|_{\tilde{x}} + \rho_f (\mathbf{u}_f - \partial_t \mathbf{d}_f|_{\tilde{x}}) \cdot \nabla \mathbf{u}_f - \operatorname{div} \sigma_f(\mathbf{u}_f, p_f) = 0 & \text{in } \Omega_f(t; \mu_g) \times [0, T], \\ \operatorname{div} \mathbf{u}_f = 0 & \text{in } \Omega_f(t; \mu_g) \times [0, T], \\ \rho_s \partial_{tt} \tilde{\mathbf{d}}_s - \operatorname{div} \tilde{\mathbf{P}}(\tilde{\mathbf{d}}_s) = 0 & \text{in } \tilde{\Omega}_s(\mu_g) \times [0, T]. \end{cases}$$

Here we notice that, again, the fluid problem is formulated in the current parametrized configuration $\Omega_f(t; \mu_g)$, whereas the solid problem is formulated in the parametrized reference configuration $\tilde{\Omega}_s(\mu_g)$. The quantity $\partial_t \mathbf{u}_f|_{\tilde{x}}$ represents the ALE time derivative: $\partial_t \mathbf{u}_f(\mathbf{x}, t; \mu_g)|_{\tilde{x}} = \partial_t \tilde{\mathbf{u}}_f(\tilde{\mathbf{x}}, t; \mu_g)$. Again, σ_f is the fluid Cauchy stress tensor, and $\tilde{\mathbf{P}}$ is the second Piola–Kirchhoff stress tensor: their definition has been given in Section 3. The previous system is completed by some suitable initial conditions, by some boundary conditions and by the following coupling conditions:

$$\begin{cases} \mathbf{d}_f = \mathbf{d}_s & \text{on } \Gamma_{FSI}(t; \mu_g) \\ \mathbf{u}_f = \partial_t \mathbf{d}_s & \text{on } \Gamma_{FSI}(t; \mu_g), \\ \tilde{J}_{\mu_g} \tilde{\sigma}_f(\tilde{\mathbf{u}}_f, \tilde{p}_f) \tilde{\mathbf{F}}_{\mu_g}^{-T} \tilde{\mathbf{n}}_f = -\tilde{\mathbf{P}}(\tilde{\mathbf{d}}_s) \tilde{\mathbf{n}}_s & \text{on } \tilde{\Gamma}_{FSI}(\mu_g), \end{cases}$$

being $\tilde{\sigma}_f$ the Cauchy stress tensor in the parametrized intermediate fluid domain $\tilde{\Omega}_f(\mu_g)$:

$$\tilde{\sigma}_f(\tilde{\mathbf{u}}_f, \tilde{p}_f) = \mu_f (\tilde{\nabla} \tilde{\mathbf{u}}_f \tilde{\mathbf{F}}_{\mu_g}^{-1} + \tilde{\mathbf{F}}_{\mu_g}^{-T} \tilde{\nabla}^T \tilde{\mathbf{u}}_f).$$

Thanks to the introduction of the pull-back maps, we can reformulate our problem in the reference configuration $\hat{\Omega}$: for every $t \in [0, T]$ and for every $\mu_g \in \mathcal{P}$, find the fluid velocity $\hat{\mathbf{u}}_f(t, \mu_g) : \hat{\Omega}_f \mapsto \mathbb{R}^2$, the fluid pressure $\hat{p}_f(t, \mu_g) : \hat{\Omega}_f \mapsto \mathbb{R}$, the fluid displacement $\hat{\mathbf{d}}_f(t, \mu_g) : \hat{\Omega}_f \mapsto \mathbb{R}^2$ and the solid deformation $\hat{\mathbf{d}}_s(t, \mu_g) : \hat{\Omega}_s \mapsto \mathbb{R}^2$ such that:

$$(17) \quad \begin{cases} \rho_f J_{\mu_g} K_{\mu_g} (\partial_t \hat{\mathbf{u}}_f + \hat{\nabla} \hat{\mathbf{u}}_f \mathbf{G}_{\mu_g}^{-1} \mathbf{F}_{\mu_g}^{-1} (\hat{\mathbf{u}}_f - \partial_t \hat{\mathbf{d}}_f)) - \\ - \operatorname{div} (J_{\mu_g} K_{\mu_g} \hat{\sigma}_f(\hat{\mathbf{u}}_f, \hat{p}_f) \mathbf{F}_{\mu_g}^{-T} \mathbf{G}_{\mu_g}^{-T}) = 0 & \text{in } \hat{\Omega}_f \times (0, T], \\ \hat{\operatorname{div}} (J_{\mu_g} K_{\mu_g} \mathbf{G}_{\mu_g}^{-1} \mathbf{F}_{\mu_g}^{-1} \hat{\mathbf{u}}_f) = 0 & \text{in } \hat{\Omega}_f \times (0, T], \\ - \hat{\operatorname{div}} (K_{\mu_g} \hat{\nabla} \hat{\mathbf{d}}_f \mathbf{G}_{\mu_g}^{-1} \mathbf{G}_{\mu_g}^{-T}) = 0 & \text{in } \hat{\Omega}_f \times (0, T], \\ \rho_s K_{\mu_g} \partial_{tt} \hat{\mathbf{d}}_s - \operatorname{div} (K_{\mu_g} \hat{\mathbf{P}}(\hat{\mathbf{d}}_s) \mathbf{G}_{\mu_g}^{-T}) = 0 & \text{in } \hat{\Omega}_s \times (0, T], \end{cases}$$

where:

$$(18) \quad \begin{aligned} \hat{\sigma}_f(\hat{\mathbf{u}}_f, \hat{p}_f) &= \mu_f (\hat{\nabla} \hat{\mathbf{u}}_f \mathbf{G}_{\mu_g}^{-1} \mathbf{F}_{\mu_g}^{-1} + \mathbf{F}_{\mu_g}^{-T} \mathbf{G}_{\mu_g}^{-T} \hat{\nabla}^T \hat{\mathbf{u}}_f), \\ \hat{\mathbf{P}}(\hat{\mathbf{d}}_s) &= \lambda_s \operatorname{tr} \varepsilon_s(\hat{\mathbf{d}}_s) \mathbf{I} + 2\mu_s \varepsilon_s(\hat{\mathbf{d}}_s), \\ \varepsilon_s(\hat{\mathbf{d}}_s) &= \frac{1}{2} (\hat{\nabla} \hat{\mathbf{d}}_s \mathbf{G}_{\mu_g}^{-1} + \mathbf{G}_{\mu_g}^{-T} \hat{\nabla}^T \hat{\mathbf{d}}_s). \end{aligned}$$

We have the coupling conditions

$$(19) \quad \begin{cases} \hat{\mathbf{d}}_f = \hat{\mathbf{d}}_s & \text{on } \hat{\Gamma}_{FSI} \\ \hat{\mathbf{u}}_f = \partial_t \hat{\mathbf{d}}_s & \text{on } \hat{\Gamma}_{FSI}, \\ J_{\mu_g} K_{\mu_g} \hat{\sigma}_f(\hat{\mathbf{u}}_f, \hat{p}_f) \mathbf{F}_{\mu_g}^{-T} \mathbf{G}_{\mu_g}^{-T} \hat{\mathbf{n}}_f = -K_{\mu_g} \hat{\mathbf{P}}(\hat{\mathbf{d}}_s) \mathbf{G}_{\mu_g}^{-T} \hat{\mathbf{n}}_s & \text{on } \hat{\Gamma}_{FSI}, \end{cases}$$

and the following boundary conditions:

$$\begin{cases} \hat{\sigma}_f(\hat{\mathbf{u}}_f, \hat{p}_f) \hat{\mathbf{n}} = -p_{in}(t) \hat{\mathbf{n}} & \text{on } \hat{\Gamma}_{in}, \\ \hat{\sigma}_f(\hat{\mathbf{u}}_f, \hat{p}_f) \hat{\mathbf{n}} = 0 & \text{on } \hat{\Gamma}_{out}, \\ \hat{\mathbf{d}}_s = 0 & \text{on } \hat{\Gamma}_s^D. \end{cases}$$

Again, $\hat{\mathbf{n}}$ represents the normal vector to the relative part of the boundary of the domain.

Remark 4.1. In this section we stressed the difference between entities on the current configuration, the parametrized intermediate configuration and the reference configuration, by using the superscripts $\tilde{\cdot}$ and $\hat{\cdot}$. However, since from now on everything will be cast in the reference configuration, and in order to make the notation as light as possible, we will drop all the superscripts.

4.3. Offline computational phase. Hereafter we present the offline phase of the partitioned procedure in the presence of a parameter μ_g . We employ again a Chorin-Temam projection scheme for the Navier–Stokes equation. Since the whole procedure is very similar to the one already presented for the non-parametric case, we present directly the final algorithm. In order to do so, we define a timestepping procedure by sampling the time interval $[0, T]$ with an equispaced sampling $\{t_0, \dots, t_{N_T}\}$, where $t_i = i\Delta T$, for $i = 0, \dots, N_T$ and $N_T = \frac{T}{\Delta T}$. We discretize the time derivative of a function f with a first backward difference: $D_t f^{i+1} = \frac{f^{i+1} - f^i}{\Delta T}$, and $D_{tt} f^{i+1} = D_t(D_t f^{i+1})$, where $f^{i+1} = f(t^{i+1})$.

In the following, we use the same function spaces that we have introduced in Section 3.2.2:

$$\begin{aligned} V(\Omega_f) &:= [H^1(\Omega_f)]^2, \\ E^f(\Omega_f) &:= [H^1(\Omega_f)]^2, \\ Q(\Omega_f) &:= L^2(\Omega_f), \\ E^s(\Omega_s) &:= [H^1(\Omega_s)]^2, \end{aligned}$$

endowed with the H^1 norm ($V(\Omega_f)$, $E^f(\Omega_f)$ and $E^s(\Omega_s)$) and the L^2 norm respectively. We remark that in the previous definitions, the domains Ω_f and Ω_s are the *reference configurations* (both parameter- and time-independent). Again we discretize in space the FSI problem, using second order Lagrange Finite Elements for fluid velocity, the fluid displacement and the solid displacement, resulting in the discrete spaces $V_h \subset V$, $E_h^f \subset E^f$ and $E_h^s \subset E^s$, while the fluid pressure is discretized with first order Lagrange Finite Elements, resulting in the discrete space $Q_h \subset Q$; we make again use of a lifting function for the fluid pressure, thus we introduce also the discrete space Q_h^0 , which is defined exactly as in Section 3.2.2.

Remark 4.2. In this case the lifting function $\ell(t)$ does not depend on the parameter μ_g , as we can deduce from the fact that the quantity $p_{in}(t)$ is parameter-independent. Therefore we can compute the lifting function, during the offline phase, *once and for all* for every timestep t^i .

The space discretized version of the partitioned procedure now reads as follows: for $i = 0, \dots, N_T$, for $\mu_g \in \mathcal{P}$:

Extrapolation of the mesh displacement: find $\mathbf{d}_{f,h}^{i+1} \in E_h^f$ such that $\forall \mathbf{e}_{f,h} \in E_h^f$:

$$(20) \quad \begin{cases} \int_{\Omega_f} K_{\mu_g} \nabla \mathbf{d}_{f,h}^{i+1} \mathbf{G}_{\mu_g}^{-1} \cdot \nabla \mathbf{e}_{f,h} \mathbf{G}_{\mu_g}^{-1} dx = 0 \\ \mathbf{d}_{f,h}^{i+1} = \mathbf{d}_{s,h}^i \quad \text{on } \Gamma_{FSI}. \end{cases}$$

Fluid explicit step: find $\mathbf{u}_{f,h}^{i+1} \in V_h$ such that $\forall \mathbf{v}_h \in V_h$:

$$(21) \quad \begin{cases} \rho_f \int_{\Omega_f} J_{\mu_g} K_{\mu_g} \left(\frac{\mathbf{u}_{f,h}^{i+1} - \mathbf{u}_{f,h}^i}{\Delta T} \right) \cdot \mathbf{v}_h dx + \\ + \rho_f \int_{\Omega_f} J_{\mu_g} K_{\mu_g} [\nabla \mathbf{u}_{f,h}^{i+1} \mathbf{G}_{\mu_g}^{-1} \mathbf{F}_{\mu_g}^{-1}] (\mathbf{u}_{f,h}^{i+1} - D_t \mathbf{d}_{f,h}^{i+1}) \cdot \mathbf{v}_h dx \\ + \mu_f \int_{\Omega_f} J_{\mu_g} K_{\mu_g} \varepsilon(\mathbf{u}_{f,h}^{i+1}) \mathbf{F}_{\mu_g}^{-T} \mathbf{G}_{\mu_g}^{-T} : \nabla \mathbf{v}_h dx + \int_{\Omega_f} J_{\mu_g} K_{\mu_g} \mathbf{F}_{\mu_g}^{-T} \mathbf{G}_{\mu_g}^{-T} \nabla p_{f,h}^i \cdot \mathbf{v}_h dx = 0 \\ \mathbf{u}_{f,h}^{i+1} = D_t \mathbf{d}_{f,h}^{i+1} \quad \text{on } \Gamma_{FSI}, \end{cases}$$

Implicit step: for any $j = 0, \dots$ until convergence:

- (1) **fluid projection substep (pressure Poisson formulation)**: find $p_{f,h}^{0,i+1,j+1} \in Q_h$ such that $\forall q_h \in Q_h^0$:

$$\begin{aligned} & \alpha_{ROB} \int_{\Gamma_{FSI}} p_{f,h}^{0,i+1,j+1} q_h ds + \int_{\Omega_f} J_{\mu_g} K_{\mu_g} \mathbf{F}_{\mu_g}^{-T} \mathbf{G}_{\mu_g}^{-T} \nabla p_{f,h}^{0,i+1,j+1} \cdot \mathbf{F}_{\mu_g}^{-T} \mathbf{G}_{\mu_g}^{-T} \nabla q_h dx = \\ & - \frac{\rho_f}{\Delta T} \int_{\Omega_f} \operatorname{div}(J_{\mu_g} K_{\mu_g} \mathbf{F}_{\mu_g}^{-1} \mathbf{G}_{\mu_g}^{-1} \mathbf{u}_{f,h}^{i+1}) q_h dx + \alpha_{ROB} \int_{\Gamma_{FSI}} p_{f,h}^{i+1,j} q_h ds \\ & - \alpha_{ROB} \int_{\Omega_f} \ell^{i+1} \cdot q_h dx - \rho_f \int_{\Gamma_{FSI}} (D_{tt} \mathbf{d}_{s,h}^{i+1,j}) \cdot J_{\mu_g} K_{\mu_g} \mathbf{F}_{\mu_g}^{-T} \mathbf{G}_{\mu_g}^{-T} \mathbf{n}_f q_h ds \\ & - \int_{\Omega_f} J_{\mu_g} K_{\mu_g} \mathbf{F}_{\mu_g}^{-T} \mathbf{G}_{\mu_g}^{-T} \nabla \ell^{i+1} \cdot \mathbf{F}_{\mu_g}^{-T} \mathbf{G}_{\mu_g}^{-T} \nabla q_h dx \end{aligned}$$

subject to the boundary conditions (7). We then retrieve the original fluid pressure $p_{f,h}^{i+1,j+1} = p_{f,h}^{0,i+1,j+1} + \ell^{i+1}$.

- (2) **structure projection substep**: find $\mathbf{d}_{s,h}^{i+1,j+1} \in E_h^s$ such that $\forall \mathbf{e}_{s,h} \in E_h^s$:

$$\begin{aligned} & \rho_s \int_{\Omega_s} K_{\mu_g} D_{tt} \mathbf{d}_{s,h}^{i+1,j+1} \cdot \mathbf{e}_{s,h} dx + \int_{\Omega_s} K_{\mu_g} \mathbf{P}(\mathbf{d}_{s,h}^{i+1,j+1}) \mathbf{G}_{\mu_g}^{-T} : \nabla \mathbf{e}_{s,h} dx = \\ & = - \int_{\Gamma_{FSI}} J_{\mu_g} K_{\mu_g} \sigma_f(\mathbf{u}_{f,h}^{i+1,j+1}, p_{f,h}^{i+1,j+1}) \mathbf{F}_{\mu_g}^{-T} \mathbf{G}_{\mu_g}^{-T} \mathbf{n}_f \cdot \mathbf{e}_{s,h} dx \end{aligned}$$

subject to the boundary condition $\mathbf{d}_{s,h}^{i+1,j+1} = 0$ on Γ_D^s

In the fluid projection step, in order to enhance the stability of the method we have employed again a Robin boundary condition, which in the case of shape parametrization reads as follows:

$$(22) \quad \begin{aligned} & \alpha_{ROB} p^{i+1} + \mathbf{F}_{\mu_g}^{-T} \mathbf{G}_{\mu_g}^{-T} \nabla p^{i+1} \cdot J_{\mu_g} K_{\mu_g} \mathbf{F}_{\mu_g}^{-T} \mathbf{G}_{\mu_g}^{-T} \mathbf{n}_f = \\ & = \alpha_{ROB} p^{i+1,*} - \rho_f D_{tt} \mathbf{d}_s^{i+1,*} \cdot J_{\mu_g} K_{\mu_g} \mathbf{F}_{\mu_g}^{-T} \mathbf{G}_{\mu_g}^{-T} \mathbf{n}_f. \end{aligned}$$

4.3.1. *POD-Greedy procedure*. In order to find the reduced basis, we rely on a POD-Greedy procedure [14, 18]: we therefore explore the parameter space \mathcal{P} with a Greedy procedure, and we explore in time with a POD. Since we do not have an a posteriori error estimator for FSI problems, and since it is beyond the scope of this work to define one, to generate the samples in the parameter space we use a *pseudo-Greedy* procedure: we sample \mathcal{P} with M equispaced points, thus obtaining the training set $\mathcal{P}_{train} = \{\mu_g^1, \dots, \mu_g^M\}$. We therefore have the following snapshots matrices:

$$\begin{aligned} \mathcal{S}_z &= [z_h(t^1; \mu_g^1), \dots, z_h(t^{N_T}; \mu_g^1), \dots, z_h(t^1; \mu_g^M), \dots, z_h(t^{N_T}; \mu_g^M)] \in \mathbb{R}^{\mathcal{N}_u^h \times \widehat{M}}, \\ \mathcal{S}_{d_s} &= [d_{s,h}(t^1, \mu_g^1), \dots, d_{s,h}(t^{N_T}, \mu_g^1), \dots, d_{s,h}(t^1, \mu_g^M), \dots, d_{s,h}(t^{N_T}, \mu_g^M)] \in \mathbb{R}^{\mathcal{N}_{d_s}^h \times \widehat{M}}, \\ \mathcal{S}_p &= [p_{f,h}^0(t^1, \mu_g^1), \dots, p_{f,h}^0(t^{N_T}, \mu_g^1), \dots, p_{f,h}^0(t^1, \mu_g^M), \dots, p_{f,h}^0(t^{N_T}, \mu_g^M)] \in \mathbb{R}^{\mathcal{N}_p^h \times \widehat{M}}, \end{aligned}$$

where $\widehat{M} = N_T \cdot M$. We perform a POD on each snapshots matrix, obtaining the following modes: $\{\Phi_z^k\}_{k=1}^{N_z}$, $\{\Phi_{d_s}^k\}_{k=1}^{N_d}$, $\{\Phi_p^k\}_{k=1}^{N_p}$, with N_z , N_d , N_p chosen according to the rate of decay of the eigenvalues returned by the POD on \mathcal{S}_z , \mathcal{S}_{d_s} and \mathcal{S}_p , respectively. We denote by V_N , E_N^s , Q_N^0 the reduced spaces spanned by these basis functions respectively. The reduced solutions $z_{f,N}^{i+1}(\mu_g)$, $p_{f,N}^{0,i+1}(\mu_g)$

and $\mathbf{d}_{s,N}^{i+1}(\mu_g)$ at timestep $i + 1$ and for $\mu_g \in \mathcal{P}$ are defined as follows:

$$(23) \quad \mathbf{z}_{f,N}^{i+1}(\mu_g) = \sum_{k=1}^{N_z} \underline{\mathbf{z}}_k^{i+1}(\mu_g) \Phi_{\mathbf{z}_f}^k,$$

$$(24) \quad p_{f,N}^{0,i+1}(\mu_g) = \sum_{k=1}^{N_p} \underline{p}_k^{0,i+1}(\mu_g) \Phi_p^k,$$

$$(25) \quad \mathbf{d}_{s,N}^{i+1}(\mu_g) = \sum_{k=1}^{N_d} \underline{\mathbf{d}}_k^{i+1}(\mu_g) \Phi_{\mathbf{d}_s}^k,$$

Remark 4.3. We remark that also in the case of parameter dependence, we implement an harmonic extension of the reduced basis for the solid displacement. Once we have the mesh displacement reduced basis $\{\Phi_{\mathbf{d}_f}^k\}_{k=1}^{N_d}$ and the relative reduced space E_N^f , we define the reduced mesh displacement as in (15).

Remark 4.4. Also in this case, if we have a non-homogeneous boundary condition for the fluid pressure, we take care of it with a lifting function ℓ , exactly as it has been done for the previous test case; however, we will not write it explicitly in the formulation, in order to ease the notation.

4.4. Online computational phase. The online phase in the case of shape parametrization is similar to the online phase described in Section 3.3; indeed, for the reduced basis generation we adopted the same strategy: we relied on a change of variable for the fluid velocity, and on an harmonic extension of the solid displacement reduced basis to obtain the reduced basis for the mesh displacement. The reduced problem now reads: for every $i = 0, \dots, N_T$ and for $\mu_g \in \mathcal{P}$:

Mesh displacement: let $\mathbf{d}_{f,N}^{i+1}(\mu_g)$ be defined by the reduced solid displacement at the previous timestep:

$$(26) \quad \mathbf{d}_{f,N}^{i+1}(\mu_g) = \sum_{k=1}^{N_d} \underline{\mathbf{d}}_k^i(\mu_g) \Phi_{\mathbf{d}_f}^k;$$

Fluid explicit step (with change of variable): find $\mathbf{z}_{f,N}^{i+1}(\mu_g) \in V_N$ such that $\forall \mathbf{v}_N \in V_N$:

$$\begin{aligned} & \rho_f \int_{\Omega_f} J_{\mu_g} K_{\mu_g} \left(\frac{\mathbf{z}_{f,N}^{i+1}(\mu_g) - \mathbf{u}_{f,N}^i(\mu_g)}{\Delta T} \right) \cdot \mathbf{v}_N dx \\ & + \mu_f \int_{\Omega_f} J_{\mu_g} K_{\mu_g} \varepsilon(\mathbf{z}_{f,N}^{i+1}(\mu_g)) \mathbf{F}_{\mu_g}^{-T} \mathbf{G}_{\mu_g}^{-T} : \nabla \mathbf{v}_N dx \\ & + \rho_f \int_{\Omega_f} J_{\mu_g} K_{\mu_g} \nabla \mathbf{z}_{f,N}^{i+1}(\mu_g) \mathbf{G}_{\mu_g}^{-1} \mathbf{F}_{\mu_g}^{-1} \mathbf{z}_{f,N}^{i+1}(\mu_g) \cdot \mathbf{v}_N dx \\ & + \rho_f \int_{\Omega_f} J_{\mu_g} K_{\mu_g} \nabla D_t \mathbf{d}_{f,N}^{i+1}(\mu_g) \mathbf{G}_{\mu_g}^{-1} \mathbf{F}_{\mu_g}^{-1} \mathbf{z}_{f,N}^{i+1}(\mu_g) \cdot \mathbf{v}_N dx \\ & + \int_{\Omega_f} J_{\mu_g} K_{\mu_g} \mathbf{F}_{\mu_g}^{-T} \mathbf{G}_{\mu_g}^{-T} \nabla p_{f,N}^i(\mu_g) \cdot \mathbf{v}_h dx = -\rho_f \int_{\Omega_f} J_{\mu_g} K_{\mu_g} \left(\frac{D_t \mathbf{d}_{f,N}^{i+1}(\mu_g)}{\Delta T} \right) \cdot \mathbf{v}_N dx \\ & - \mu_f \int_{\Omega_f} J_{\mu_g} K_{\mu_g} \varepsilon(D_t \mathbf{d}_{f,N}^{i+1}(\mu_g)) \mathbf{F}_{\mu_g}^{-T} \mathbf{G}_{\mu_g}^{-T} : \nabla \mathbf{v}_N dx. \end{aligned}$$

We then restore the reduced fluid velocity: $\mathbf{u}_{f,N}^{i+1}(\mu_g) = \mathbf{z}_{f,N}^{i+1}(\mu_g) + D_t \mathbf{d}_{f,N}^{i+1}(\mu_g)$.

Implicit step: for any $j = 0, \dots$ until convergence:

(1) **fluid projection substep:** find $p_{f,N}^{0,i+1,j+1}(\mu_g) \in Q_N^0$ such that $\forall q_N \in Q_N^0$:

$$\begin{aligned} & \alpha_{ROB} \int_{\Gamma_{FSI}} p_{f,N}^{0,i+1,j+1}(\mu_g) q_N ds + \\ & + \int_{\Omega_f} J_{\mu_g} K_{\mu_g} \mathbf{F}_{\mu_g}^{-T} \mathbf{G}_{\mu_g}^{-T} \nabla p_{f,N}^{0,i+1,j+1}(\mu_g) \cdot \mathbf{F}_{\mu_g}^{-T} \mathbf{G}_{\mu_g}^{-T} \nabla q_N dx = \\ & - \frac{\rho_f}{\Delta T} \int_{\Omega_f} \operatorname{div}(J_{\mu_g} K_{\mu_g} \mathbf{G}_{\mu_g}^{-1} \mathbf{F}_{\mu_g}^{-1} \mathbf{u}_{f,N}^{i+1}(\mu_g)) q_N dx + \alpha_{ROB} \int_{\Gamma_{FSI}} p_{f,N}^{i+1,j}(\mu_g) q_N ds - \\ & - \alpha_{ROB} \int_{\Gamma_{FSI}} \ell_N^{i+1} \cdot q_N dx - \rho_f \int_{\Gamma_{FSI}} D_{tt} \mathbf{d}_{s,N}^{i+1,j}(\mu_g) \cdot J_{\mu_g} K_{\mu_g} \mathbf{F}_{\mu_g}^{-T} \mathbf{G}_{\mu_g}^{-T} \mathbf{n}_f q_N ds - \\ & - \int_{\Omega_f} J_{\mu_g} K_{\mu_g} \mathbf{F}_{\mu_g}^{-T} \mathbf{G}_{\mu_g}^{-T} \nabla \ell_N^{i+1} \cdot \mathbf{F}_{\mu_g}^{-T} \mathbf{G}_{\mu_g}^{-T} \nabla q_N dx, \end{aligned}$$

where ℓ_N^{i+1} is the projection of ℓ^{i+1} onto the reduced order space Q_N . We then recover the reduced order fluid pressure $p_{f,N}^{i+1,j+1} = p_{f,N}^{0,i+1,j+1} + \ell_N^{i+1}$.

(2) **structure projection substep:** find $\mathbf{d}_{s,N}^{i+1,j+1}(\mu_g) \in E_N^s$ such that $\forall \mathbf{e}_s \in E_N^s$:

$$\begin{aligned} & \rho_s \int_{\Omega_s} K_{\mu_g} D_{tt} \mathbf{d}_{s,N}^{i+1,j+1}(\mu_g) \cdot \mathbf{e}_N dx + \int_{\Omega_s} K_{\mu_g} \mathbf{P}(\mathbf{d}_{s,N}^{i+1,j+1}(\mu_g)) \mathbf{G}_{\mu_g}^{-T} : \nabla \mathbf{e}_N dx = \\ & = - \int_{\Omega_s} J_{\mu_g} K_{\mu_g} \sigma_f(\mathbf{u}_{f,N}^{i+1}(\mu_g), p_{f,N}^{i+1,j+1}(\mu_g)) \mathbf{F}_{\mu_g}^{-T} \mathbf{G}_{\mu_g}^{-T} \mathbf{n}_f \cdot \mathbf{e}_N dx. \end{aligned}$$

4.5. Numerical results. We now present some numerical results concerning the parametrized version of the two dimensional FSI test case presented in Section 3. The original domain is shown in Figure 7, together with the reference configuration, and the parametrized reference configuration. The fluid domain is represented in blue, while the solid (the leaflets) is depicted in red. The height of the channel is 2.5 cm, its length is 10 cm; the leaflets are 0.2 cm thick, and they are situated 1 cm downstream the fluid inlet, which corresponds to the vertical boundary on the left of the blue domain. One geometrical parameter is considered: the length μ_g of the leaflets, where we have chosen $\mu_g \in \mathcal{P} = [0.5, 1.0]$. An affine mapping T is chosen to deform the reference domain $\hat{\Omega}$, obtained for $\mu_g = 1.0$ cm, to the parametrized configuration $\tilde{\Omega}(\mu_g)$. Top and bottom walls of the blue domain are rigid, thus both the displacement \mathbf{d}_f and the fluid velocity \mathbf{u}_f are set to zero. Homogeneous Neumann condition is imposed on \mathbf{u}_f on the outlet; a pressure profile $p_{in}(t)$ is described at the inlet, where:

$$p_{in}(t) = \begin{cases} 5 - 5 \cos\left(\frac{2\pi t}{T_{in}}\right) & \text{for } t \leq 0.1s \\ 5 & \text{for } t > 0.1s, \end{cases}$$

and $T_{in} = 0.4$ s. Also in this case we set a tolerance of $\varepsilon = 10^{-6}$ as a stopping criterion for the subiterations between the pressure problem and the solid problem.

For the simulation, we use a timestep $\Delta t = 10^{-4}$, for a maximum number of timesteps $N_T = 800$, thus $T = 0.08s$. Table 2 summarizes the details of the offline stage and of the FE discretization.

Figure 8a shows the rate of decay of the eigenvalues returned by a POD on \mathbf{z}_f , p_f and \mathbf{d}_s , respectively. As we can see, now the eigenvalues of the pressure decay faster than the ones for the displacement and for the fluid velocity. This is confirmed also at the level of retained energy, as we can see from Figure 8b: the first mode of the pressure is indeed the most energetic one, while the first mode of the velocity is the least energetic one. In Figure 9 we see a representative solution for the fluid velocity, for two different values of the geometrical parameter μ_g . As we can notice, for the same inlet pressure profile, when the leaflets are longer, at the final time of the simulation ($T = 0.08s$) we are close to the formation of a jet inbetween the two leaflets. Figure 10 shows the reduced displacement, for the three different values of the geometrical parameter: $\mu_g = 0.61$, $\mu_g = 0.78$ and $\mu_g = 1.0$; the influence of μ_g is clear: the longer the leaflets, the bigger their deformation is going to be, under the same physical parameters.

TABLE 2. Physical and geometrical constants and parameters, for the geometrically parametrized leaflets test case.

Physical parameter	Value
ρ_s	1.1 g/cm ³
μ_s	100000
λ_s	800000
ρ_f	1 g/cm ³
μ_f	0.035 Poise
Geometrical parameter	Value
μ_g	[0.5, 1.0]
FE displacement order	2
FE velocity order	2
FE pressure order	1
N_{train}	10
N	100

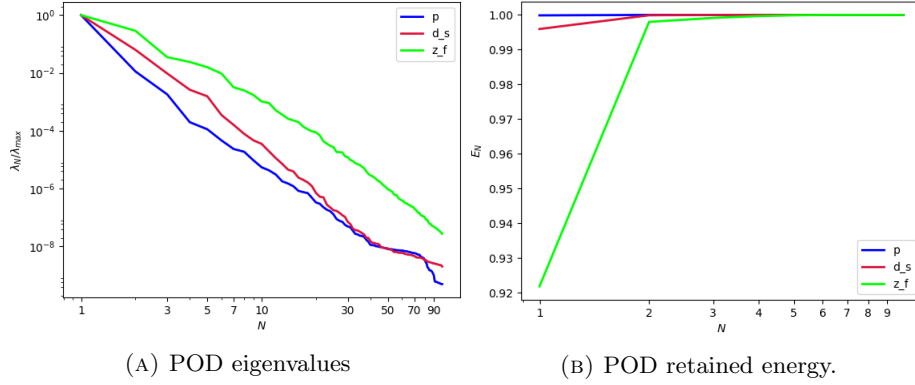


FIGURE 8. POD results for the test case with a domain with geometrical parametrization.

5. THIRD TEST CASE: SHAPE PARAMETRIZATION AND PHYSICAL PARAMETRIZATION

As a last test case, we consider the geometrically parametrized version of the problem of interest, and we add to the formulation a physical parameter μ_s , which represents the shear modulus of the material of which the leaflets are made of. Let us denote by $\boldsymbol{\mu} = (\mu_g, \mu_s)$ the parameter vector, with $\boldsymbol{\mu} \in \mathcal{P} \subset \mathbb{R}^2$, where $\mathcal{P} := [\mu_g^{min}, \mu_g^{max}] \times [\mu_s^{min}, \mu_s^{max}]$ is the parameter domain.

5.1. Strong formulation. The strong formulation, in the current configuration, reads as follows: for every $t \in [0, T]$ and for every $\boldsymbol{\mu} \in \mathcal{P}$, find $\mathbf{u}_f(t; \boldsymbol{\mu}): \Omega_f(t; \boldsymbol{\mu}) \mapsto \mathbb{R}^2$, the fluid pressure $p_f(t; \boldsymbol{\mu}): \Omega_f(t; \boldsymbol{\mu}) \mapsto \mathbb{R}$, the mesh displacement $\tilde{\mathbf{d}}_f(t; \boldsymbol{\mu}): \tilde{\Omega}_f(\boldsymbol{\mu}) \mapsto \mathbb{R}^2$ and the solid displacement $\tilde{\mathbf{d}}_s(t; \boldsymbol{\mu}): \tilde{\Omega}_s(\boldsymbol{\mu}) \mapsto \mathbb{R}^2$ such that:

$$\begin{cases} -\tilde{\Delta} \tilde{\mathbf{d}}_f = 0 & \text{in } \tilde{\Omega}_f(\boldsymbol{\mu}) \times [0, T], \\ \tilde{\mathbf{d}}_f = \tilde{\mathbf{d}}_s & \text{on } \tilde{\Gamma}_{FSI} \times [0, T], \end{cases}$$

and

$$\begin{cases} \rho_f \partial_t \mathbf{u}_f|_{\tilde{x}} + \rho_f (\mathbf{u}_f - \partial_t \tilde{\mathbf{d}}_f|_{\tilde{x}}) \cdot \nabla \mathbf{u}_f - \operatorname{div} \sigma_f(\mathbf{u}_f, p_f) = 0 & \text{in } \Omega_f(t; \boldsymbol{\mu}) \times [0, T], \\ \operatorname{div} \mathbf{u}_f = 0 & \text{in } \Omega_f(t; \boldsymbol{\mu}) \times [0, T], \\ \rho_s \partial_{tt} \tilde{\mathbf{d}}_s - \operatorname{div} \tilde{\mathbf{P}}(\tilde{\mathbf{d}}_s, \mu_s) = 0 & \text{in } \tilde{\Omega}_s(\boldsymbol{\mu}) \times [0, T], \end{cases}$$

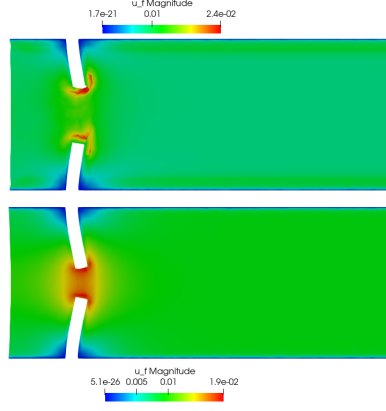


FIGURE 9. Representative solutions for the fluid velocity \mathbf{u}_f , obtained with the reduced order model proposed ($N_z = 100$ basis for the fluid velocity), for different values of the leaflet length μ_g : $\mu_g = 0.77$ (top), and $\mu_g = 1.0$ (bottom).



FIGURE 10. Representative solutions for the displacement of the leaflets, \mathbf{d}_s , obtained with the reduced order model proposed ($N_d = 100$ basis for the displacement), for different values of the leaflet length μ_g : $\mu_g = 0.61$ (left), $\mu_g = 0.78$ (center), and $\mu_g = 1.0$ (right). The displacement has been magnified by a factor 10^3 for visualization purposes.

where now the second Piola–Kirchhoff stress tensor $\tilde{\mathbf{P}}$ in the intermediate configuration depends also on the physical parameter μ_s :

$$\tilde{\mathbf{P}}(\tilde{\mathbf{d}}_s, \mu_s) := \lambda_s \text{tr} \varepsilon_s(\tilde{\mathbf{d}}_s) + 2\mu_s \varepsilon(\tilde{\mathbf{d}}_s), \quad \mu_s \in [\mu_s^{\min}, \mu_s^{\max}].$$

The coupling conditions are the same as in (19), and, thanks to the pullback maps already introduced in Section 4, we can formulate the problem in the reference configuration $\hat{\Omega}$. For every $t \in [0, T]$, and for every $\boldsymbol{\mu} \in \mathcal{P}$, find the fluid velocity $\hat{\mathbf{u}}_f(t, \boldsymbol{\mu}) : \hat{\Omega}_f \mapsto \mathbb{R}^2$, the fluid pressure $\hat{p}_f(t, \boldsymbol{\mu}) : \hat{\Omega}_f \mapsto \mathbb{R}$, the mesh displacement $\hat{\mathbf{d}}_f(t, \boldsymbol{\mu}) : \hat{\Omega}_f \mapsto \mathbb{R}^2$ and the solid deformation $\hat{\mathbf{d}}_s(t, \boldsymbol{\mu}) : \hat{\Omega}_s \mapsto \mathbb{R}^2$ such that:

$$(27) \quad \begin{cases} \rho_f J_{\mu_g} K_{\mu_g} (\partial_t \hat{\mathbf{u}}_f + \hat{\nabla} \hat{\mathbf{u}}_f \mathbf{G}_{\mu_g}^{-1} \mathbf{F}_{\mu_g}^{-1} (\hat{\mathbf{u}}_f - \partial_t \hat{\mathbf{d}}_f)) - \\ - \hat{\text{div}}(J_{\mu_g} K_{\mu_g} \hat{\sigma}_f(\hat{\mathbf{u}}_f, \hat{p}_f) \mathbf{F}_{\mu_g}^{-T} \mathbf{G}_{\mu_g}^{-T}) = 0 \quad \text{in } \hat{\Omega}_f \times (0, T], \\ \hat{\text{div}}(J_{\mu_g} K_{\mu_g} \mathbf{G}_{\mu_g}^{-1} \mathbf{F}_{\mu_g}^{-1} \hat{\mathbf{u}}_f) = 0 \quad \text{in } \hat{\Omega}_f \times (0, T], \\ - \hat{\text{div}}(K_{\mu_g} \hat{\nabla} \hat{\mathbf{d}}_f \mathbf{G}_{\mu_g}^{-1} \mathbf{G}_{\mu_g}^{-T}) = 0 \quad \text{in } \hat{\Omega}_f \times (0, T], \\ \rho_s K_{\mu_g} \partial_{tt} \hat{\mathbf{d}}_s - \hat{\text{div}}(K_{\mu_g} \hat{\mathbf{P}}(\hat{\mathbf{d}}_s, \mu_s) \mathbf{G}_{\mu_g}^{-T}) = 0 \quad \text{in } \hat{\Omega}_s \times (0, T], \end{cases}$$

where:

$$\begin{aligned}
\hat{\sigma}_f(\hat{\mathbf{u}}_f, \hat{p}_f) &= \mu_f(\hat{\nabla}\hat{\mathbf{u}}_f\mathbf{G}_{\mu_g}^{-1}\mathbf{F}_{\mu_g}^{-1} + \mathbf{F}_{\mu_g}^{-T}\mathbf{G}_{\mu_g}^{-T}\hat{\nabla}^T\hat{\mathbf{u}}_f), \\
\hat{\mathbf{P}}(\hat{\mathbf{d}}_s, \mu_s) &= \lambda_s \text{tr}\varepsilon_s(\hat{\mathbf{d}}_s)\mathbf{I} + 2\mu_s\varepsilon_s(\hat{\mathbf{d}}_s), \quad \mu_s \in [\mu_s^{\min}, \mu_s^{\max}] \\
(28) \quad \varepsilon_s(\hat{\mathbf{d}}_s) &= \frac{1}{2}(\hat{\nabla}\hat{\mathbf{d}}_s\mathbf{G}_{\mu_g}^{-1} + \mathbf{G}_{\mu_g}^{-T}\hat{\nabla}^T\hat{\mathbf{d}}_s).
\end{aligned}$$

System (27) is completed by the usual coupling conditions and by some suitable initial and boundary conditions.

Remark 5.1. Again, in order to ease the notation and the exposition, in the following we are going to drop the notation with the $\hat{\cdot}$, since everything is intended to be taken in the reference configuration $\hat{\Omega}$.

5.2. Offline computational phase: reduced basis generation. We are now going to present the offline computational phase of the algorithm. We start by discretizing the time interval $[0, T]$ with $\{0 = t_0, \dots, t_{N_T} = T\}$, where $t_i = i\Delta T$ for $i = 0, \dots, N_T$. We then discretize the parameter space $\mathcal{P} = [\mu_g^{\min}, \mu_g^{\max}] \times [\mu_s^{\min}, \mu_s^{\max}]$ with an equispaced sampling, and we obtain $\mathcal{P}_{train} = [\mu_g^1, \dots, \mu_g^{M_g}] \times [\mu_s^1, \dots, \mu_s^{M_s}]$. The offline phase of the algorithm is the same as for the geometrically parametrized test case: we use the same discrete spaces $V_h, Q_h, Q_h^0, E_h^f, E_h^s$ previously introduced in Section 4.3. For every $\boldsymbol{\mu} = (\mu_g, \mu_s) \in \mathcal{P}_{train}$, and for $i = 0, \dots, N_T$:

Extrapolation of the mesh displacement: find $\mathbf{d}_{f,h}^{i+1} \in E_h^f$ such that $\forall \mathbf{e}_{f,h} \in E_h^f$:

$$(29) \quad \begin{cases} \int_{\Omega_f} K_{\mu_g} \nabla \mathbf{d}_{f,h}^{i+1} \mathbf{G}_{\mu_g}^{-1} \cdot \nabla \mathbf{e}_{f,h} \mathbf{G}_{\mu_g}^{-1} dx = 0 \\ \mathbf{d}_{f,h}^{i+1} = \mathbf{d}_{s,h}^i \quad \text{on } \Gamma_{FSI}. \end{cases}$$

Fluid explicit step: find $\mathbf{u}_{f,h}^{i+1} \in V_h$ such that $\forall \mathbf{v}_h \in V_h$:

$$(30) \quad \begin{cases} \rho_f \int_{\Omega_f} J_{\mu_g} K_{\mu_g} \left(\frac{\mathbf{u}_{f,h}^{i+1} - \mathbf{u}_{f,h}^i}{\Delta T} \right) \cdot \mathbf{v}_h dx + \\ + \rho_f \int_{\Omega_f} J_{\mu_g} K_{\mu_g} [\nabla \mathbf{u}_{f,h}^{i+1} \mathbf{G}_{\mu_g}^{-1} \mathbf{F}_{\mu_g}^{-1}] (\mathbf{u}_{f,h}^{i+1} - D_t \mathbf{d}_{f,h}^{i+1}) \cdot \mathbf{v}_h dx + \\ + \mu_f \int_{\Omega_f} J_{\mu_g} K_{\mu_g} \varepsilon(\mathbf{u}_{f,h}^{i+1}) \mathbf{F}_{\mu_g}^{-T} \mathbf{G}_{\mu_g}^{-T} : \nabla \mathbf{v}_h dx + \int_{\Omega_f} J_{\mu_g} K_{\mu_g} \mathbf{F}_{\mu_g}^{-T} \mathbf{G}_{\mu_g}^{-T} \nabla p_{f,h}^i \cdot \mathbf{v}_h dx = 0 \\ \mathbf{u}_{f,h}^{i+1} = D_t \mathbf{d}_{f,h}^{i+1} \quad \text{on } \Gamma_{FSI}, \end{cases}$$

Implicit step: for any $j = 0, \dots$ until convergence:

- (1) **fluid projection substep (pressure Poisson formulation):** find $p_{f,h}^{0,i+1,j+1} \in Q_h^0$ such that $\forall q_h \in Q_h^0$:

$$\begin{aligned}
\alpha_{ROB} \int_{\Gamma_{FSI}} p_{f,h}^{0,i+1,j+1} q_h ds + \int_{\Omega_f} J_{\mu_g} K_{\mu_g} \mathbf{G}_{\mu_g}^{-T} \mathbf{F}_{\mu_g}^{-T} \nabla p_{f,h}^{0,i+1,j+1} \cdot \mathbf{G}_{\mu_g}^{-T} \mathbf{F}_{\mu_g}^{-T} \nabla q_h dx = \\
- \frac{\rho_f}{\Delta T} \int_{\Omega_f} \text{div}(J_{\mu_g} K_{\mu_g} \mathbf{G}_{\mu_g}^{-1} \mathbf{F}_{\mu_g}^{-1} \mathbf{u}_{f,h}^{i+1}) q_h dx + \alpha_{ROB} \int_{\Gamma_{FSI}} p_{f,h}^{0,i+1,j} q_h ds - \\
- \alpha_{ROB} \int_{\Gamma_{FSI}} \ell^{i+1} q_h ds - \rho_f \int_{\Gamma_{FSI}} (D_{tt} \mathbf{d}_{s,h}^{i+1,j}) \cdot J_{\mu_g} K_{\mu_g} \mathbf{F}_{\mu_g}^{-T} \mathbf{G}_{\mu_g}^{-T} \mathbf{n}_f q_h ds - \\
- \int_{\Omega_f} J_{\mu_g} K_{\mu_g} \mathbf{G}_{\mu_g}^{-T} \mathbf{F}_{\mu_g}^{-T} \nabla \ell^{i+1} \cdot \mathbf{G}_{\mu_g}^{-T} \mathbf{F}_{\mu_g}^{-T} \nabla q_h dx
\end{aligned}$$

where then $p_{f,h}^{i+1,j+1} = p_{f,h}^{0,i+1,j+1} + \ell^{i+1}$.

(2) **structure projection substep:** find $\mathbf{d}_{s,h}^{i+1,j+1} \in E_h^s$ such that $\forall \mathbf{e}_{s,h} \in E_h^s$:

$$\begin{aligned} & \rho_s \int_{\Omega_s} K_{\mu_g} D_{tt} \mathbf{d}_{s,h}^{i+1,j+1} \cdot \mathbf{e}_{s,h} dx + \int_{\Omega_s} K_{\mu_g} \mathbf{P}(\mathbf{d}_{s,h}^{i+1,j+1}, \mu_s) \mathbf{G}_{\mu_g}^{-T} : \nabla \mathbf{e}_{s,h} dx = \\ & = - \int_{\Gamma_{FSI}} J_{\mu_g} K_{\mu_g} \sigma_f(\mathbf{u}_{f,h}^{i+1,j+1}, p_{f,h}^{0,i+1,j+1}) \mathbf{G}_{\mu_g}^{-T} \mathbf{F}_{\mu_g}^{-T} \mathbf{n}_f \cdot \mathbf{e}_{s,h} dx, \end{aligned}$$

subject to the boundary condition $\mathbf{d}_{s,h}^{i+1,j+1} = 0$ on Γ_D^s .

Remark 5.2. Also in this case, to enhance the stability of the fluid–solid subproblems we used Robin coupling condition (22) in the Poisson problem.

5.2.1. *POD and reduced basis generation.* For this test case we decided to adopt a POD strategy which is slightly different with respect to the standard POD that we presented for the other two test cases. Indeed, the idea here is to first perform a standard POD on the set of snapshots computed for every value of the parameter $\boldsymbol{\mu}$ in the training set \mathcal{P}_{train} . Then, afterwards, we take the modes computed with the standard POD, weighted with the corresponding eigenvalue, and we perform a final outer run of POD.

Let us now present briefly the procedure: we start by constructing, for each parameter $\boldsymbol{\mu}_{i,j} = (\mu_g^i, \mu_s^j) \in \mathcal{P}_{train}$, the snapshots matrices $\mathcal{S}_z(\boldsymbol{\mu}_{i,j})$ for the fluid change of variable \mathbf{z}_f , $\mathcal{S}_p(\boldsymbol{\mu}_{i,j})$ for the fluid pressure p_f^0 and $\mathcal{S}_{d_s}(\boldsymbol{\mu}_{i,j})$ for the solid displacement \mathbf{d}_s :

$$\begin{aligned} \mathcal{S}_z(\boldsymbol{\mu}_{i,j}) &= \{\mathbf{z}_{f,h}(t_0, \boldsymbol{\mu}_{i,j}), \dots, \mathbf{z}_{f,h}(t_{N_T}, \boldsymbol{\mu}_{i,j})\} \in \mathbb{R}^{N_u^h \times N_T}, \\ \mathcal{S}_p(\boldsymbol{\mu}_{i,j}) &= \{p_{f,h}^0(t_0, \boldsymbol{\mu}_{i,j}), \dots, p_{f,h}^0(t_{N_T}, \boldsymbol{\mu}_{i,j})\} \in \mathbb{R}^{N_p^h \times N_T}, \\ \mathcal{S}_{d_s}(\boldsymbol{\mu}_{i,j}) &= \{\mathbf{d}_{s,h}(t_0, \boldsymbol{\mu}_{i,j}), \dots, \mathbf{d}_{s,h}(t_{N_T}, \boldsymbol{\mu}_{i,j})\} \in \mathbb{R}^{N_{d_s}^h \times N_T}. \end{aligned}$$

We then perform a standard POD on each snapshots matrix and we extract the basis functions $\{\Phi_{z_f}^k(\boldsymbol{\mu}_{i,j})\}_{k=1}^{N_{z_f}^z}$, $\{\Phi_p^k(\boldsymbol{\mu}_{i,j})\}_{k=1}^{N_p^p}$ and $\{\Phi_{d_s}^k(\boldsymbol{\mu}_{i,j})\}_{k=1}^{N_{d_s}^d}$. Let us also call $\{\lambda_n^z\}_{n=1}^{N_{z_f}^z}$, $\{\lambda_n^p\}_{n=1}^{N_p^p}$, $\{\lambda_n^d\}_{n=1}^{N_{d_s}^d}$ the eigenvalues, ordered by decreasing order of magnitude, returned by the POD on each snapshot matrix $\mathcal{S}_z(\boldsymbol{\mu}_{i,j})$, $\mathcal{S}_p(\boldsymbol{\mu}_{i,j})$, $\mathcal{S}_{d_s}(\boldsymbol{\mu}_{i,j})$. Afterwards, we perform a second run of POD in the following way: we start by building the snapshots matrices always for the components \mathbf{z}_f , p_f and \mathbf{d}_s , normalizing each snapshot with the corresponding eigenvalue given by the standard POD:

$$\begin{aligned} \mathcal{S}_z &= \left\{ \frac{1}{\sqrt{\lambda_1^z}} \Phi_{z_f}^1(\boldsymbol{\mu}_{1,1}), \dots, \frac{1}{\sqrt{\lambda_{N_{z_f}^z}^z}} \Phi_{z_f}^{N_{z_f}^z}(\boldsymbol{\mu}_{1,1}), \dots, \frac{1}{\sqrt{\lambda_{N_{M_g, M_s}^z}^z}} \Phi_{z_f}^{N_{M_g, M_s}^z}(\boldsymbol{\mu}_{M_g, M_s}) \right\}, \\ \mathcal{S}_p &= \left\{ \frac{1}{\sqrt{\lambda_1^p}} \Phi_p^1(\boldsymbol{\mu}_{1,1}), \dots, \frac{1}{\sqrt{\lambda_{N_p^p}^p}} \Phi_p^{N_p^p}(\boldsymbol{\mu}_{1,1}), \dots, \frac{1}{\sqrt{\lambda_{N_{M_g, M_s}^p}^p}} \Phi_p^{N_{M_g, M_s}^p}(\boldsymbol{\mu}_{M_g, M_s}) \right\}, \\ \mathcal{S}_{d_s} &= \left\{ \frac{1}{\sqrt{\lambda_1^d}} \Phi_{d_s}^1(\boldsymbol{\mu}_{1,1}), \dots, \frac{1}{\sqrt{\lambda_{N_{d_s}^d}^d}} \Phi_{d_s}^{N_{d_s}^d}(\boldsymbol{\mu}_{1,1}), \dots, \frac{1}{\sqrt{\lambda_{N_{M_g, M_s}^d}^d}} \Phi_{d_s}^{N_{M_g, M_s}^d}(\boldsymbol{\mu}_{M_g, M_s}) \right\}. \end{aligned}$$

We then perform a second POD on the previous snapshots matrices, and we finally obtain a set of basis functions $\{\Phi_{z_f}^k\}_{k=1}^{N_{z_f}^z}$, $\{\Phi_p^k\}_{k=1}^{N_p^p}$ and $\{\Phi_{d_s}^k\}_{k=1}^{N_{d_s}^d}$. Then, to obtain a set of basis functions for the mesh displacement \mathbf{d}_f , we choose to employ again an harmonic extension of the solid displacement basis functions $\Phi_{d_s}^k$ on the entire fluid domain Ω_f , as we have done for the previous two test cases; in this way we obtain a set $\{\Phi_{d_f}^k\}_{k=1}^{N_{d_f}^d}$ of reduced basis also for the mesh displacement.

5.3. **Online phase.** The online phase of the algorithm is very similar to the online phase for the geometrically parametrized test case. We start by introducing the online solutions $\mathbf{z}_{f,N}^{i+1}$, $p_{f,N}^{i+1}$ and

$\mathbf{d}_{s,N}^{i+1}$ at timestep t^{i+1} :

$$(31) \quad \mathbf{z}_{f,N}^{i+1}(\boldsymbol{\mu}) = \sum_{k=1}^{N_z} \underline{z}_k^{i+1}(\boldsymbol{\mu}) \boldsymbol{\Phi}_{z_f}^k,$$

$$(32) \quad p_{f,N}^{0,i+1}(\boldsymbol{\mu}) = \sum_{k=1}^{N_p} \underline{p}_k^{0,i+1}(\boldsymbol{\mu}) \boldsymbol{\Phi}_p^k,$$

$$(33) \quad \mathbf{d}_{s,N}^{i+1}(\boldsymbol{\mu}) = \sum_{k=1}^{N_d} \underline{d}_k^{i+1}(\boldsymbol{\mu}) \boldsymbol{\Phi}_{d_s}^k.$$

The reduced problem then reads: for every $i = 0, \dots, N_T$ and for $\boldsymbol{\mu} = (\mu_g, \mu_s) \in \mathcal{P}$:

Mesh displacement: let $\mathbf{d}_{f,N}^{i+1}(\boldsymbol{\mu})$ be defined by the reduced solid displacement at the previous timestep:

$$(34) \quad \mathbf{d}_{f,N}^{i+1}(\boldsymbol{\mu}) = \sum_{k=1}^{N_d} \underline{d}_k^i(\boldsymbol{\mu}) \boldsymbol{\Phi}_{d_f}^k;$$

Fluid explicit step (with change of variable): find $\mathbf{z}_{f,N}^{i+1}(\boldsymbol{\mu}) \in V_N$ such that $\forall \mathbf{v}_N \in V_N$:

$$\begin{aligned} & \rho_f \int_{\Omega_f} J_{\mu_g} K_{\mu_g} \left(\frac{\mathbf{z}_{f,N}^{i+1}(\boldsymbol{\mu}) - \mathbf{u}_{f,N}^i(\boldsymbol{\mu})}{\Delta T} \right) \cdot \mathbf{v}_N \, dx + \\ & + \mu_f \int_{\Omega_f} J_{\mu_g} K_{\mu_g} \varepsilon(\mathbf{z}_{f,N}^{i+1}(\boldsymbol{\mu})) \mathbf{F}_{\mu_g}^{-T} \mathbf{G}_{\mu_g}^{-T} : \nabla \mathbf{v}_N \, dx + \\ & + \rho_f \int_{\Omega_f} J_{\mu_g} K_{\mu_g} \nabla \mathbf{z}_{f,N}^{i+1}(\boldsymbol{\mu}) \mathbf{G}_{\mu_g}^{-1} \mathbf{F}_{\mu_g}^{-1} \mathbf{z}_{f,N}^{i+1}(\boldsymbol{\mu}_g) \cdot \mathbf{v}_N \, dx + \\ & + \rho_f \int_{\Omega_f} J_{\mu_g} K_{\mu_g} \nabla D_t \mathbf{d}_{f,N}^{i+1}(\boldsymbol{\mu}) \mathbf{G}_{\mu_g}^{-1} \mathbf{F}_{\mu_g}^{-1} \mathbf{z}_{f,N}^{i+1}(\boldsymbol{\mu}) \cdot \mathbf{v}_N \, dx \\ & + \int_{\Omega_f} J_{\mu_g} K_{\mu_g} \mathbf{F}_{\mu_g}^{-T} \mathbf{G}_{\mu_g}^{-T} \nabla p_{f,N}^i(\boldsymbol{\mu}) \cdot \mathbf{v}_h \, dx = -\rho_f \int_{\Omega_f} J_{\mu_g} K_{\mu_g} \left(\frac{D_t \mathbf{d}_{f,N}^{i+1}(\boldsymbol{\mu})}{\Delta T} \right) \cdot \mathbf{v}_N \, dx - \\ & - \mu_f \int_{\Omega_f} J_{\mu_g} K_{\mu_g} \varepsilon(D_t \mathbf{d}_{f,N}^{i+1}(\boldsymbol{\mu})) \mathbf{F}_{\mu_g}^{-T} \mathbf{G}_{\mu_g}^{-T} : \nabla \mathbf{v}_N \, dx \quad \text{in } \Omega_f. \end{aligned}$$

We then restore the reduced fluid velocity: $\mathbf{u}_{f,N}^{i+1}(\boldsymbol{\mu}) = \mathbf{z}_{f,N}^{i+1}(\boldsymbol{\mu}) + D_t \mathbf{d}_{f,N}^{i+1}(\boldsymbol{\mu})$.

Implicit step: for any $j = 0, \dots$ until convergence:

(1) **fluid projection substep**: find $p_{f,N}^{0,i+1,j+1}(\boldsymbol{\mu}) \in Q_N^0$ such that $\forall q_N \in Q_N^0$:

$$\begin{aligned} & \alpha_{ROB} \int_{\Gamma_{FSI}} p_{f,N}^{0,i+1,j+1}(\boldsymbol{\mu}) q_N \, ds + \\ & + \int_{\Omega_f} J_{\mu_g} K_{\mu_g} \mathbf{F}_{\mu_g}^{-T} \mathbf{G}_{\mu_g}^{-T} \nabla p_{f,N}^{0,i+1,j+1}(\boldsymbol{\mu}) \cdot \mathbf{F}_{\mu_g}^{-T} \mathbf{G}_{\mu_g}^{-T} \nabla q_N \, dx = \\ & - \frac{\rho_f}{\Delta T} \int_{\Omega_f} \operatorname{div}(J_{\mu_g} K_{\mu_g} \mathbf{G}_{\mu_g}^{-1} \mathbf{F}_{\mu_g}^{-1} \mathbf{u}_{f,N}^{i+1}(\boldsymbol{\mu})) q_N \, dx + \alpha_{ROB} \int_{\Gamma_{FSI}} p_{f,N}^{0,i+1,j}(\boldsymbol{\mu}) q_N \, ds - \\ & - \alpha_{ROB} \int_{\Gamma_{FSI}} \ell_N^{i+1} q_N \, ds - \rho_f \int_{\Gamma_{FSI}} D_{tt} \mathbf{d}_{s,N}^{i+1,j}(\boldsymbol{\mu}) \cdot J_{\mu_g} K_{\mu_g} \mathbf{F}_{\mu_g}^{-T} \mathbf{G}_{\mu_g}^{-T} \mathbf{n}_f q_N \, ds - \\ & - \int_{\Omega_f} J_{\mu_g} K_{\mu_g} \mathbf{F}_{\mu_g}^{-T} \mathbf{G}_{\mu_g}^{-T} \nabla \ell_N^{i+1} \cdot \mathbf{F}_{\mu_g}^{-T} \mathbf{G}_{\mu_g}^{-T} \nabla q_N \, dx \end{aligned}$$

we then recover the reduced fluid pressure $p_{f,N}^{i+1,j+1} = p_{f,N}^{0,i+1,j+1} + \ell_N^{i+1}$.

TABLE 3. Physical and geometrical constants and parameters, for the geometrically and physically parametrized leaflets test case.

Physical constant	Value
ρ_s	1.1 g/cm ³
λ_s	800000
ρ_f	1 g/cm ³
μ_f	0.035 Poise
Geometrical parameter	Value
μ_g	[0.5, 1.0]
FE displacement order	2
FE velocity order	2
FE pressure order	1
N_{train}	10
N	100
Physical parameter	Value
μ_s	[10000, 80000]

(2) **structure projection substep:** find $\mathbf{d}_{s,N}^{i+1,j+1}(\boldsymbol{\mu}) \in E_N^s$ such that $\forall \mathbf{e}_s \in E_N^s$:

$$\begin{aligned} & \rho_s \int_{\Omega_s} K_{\mu_g} D_{tt} \mathbf{d}_{s,N}^{i+1,j+1}(\boldsymbol{\mu}) \cdot \mathbf{e}_N dx + \int_{\Omega_s} K_{\mu_g} \mathbf{P}(\mathbf{d}_{s,N}^{i+1,j+1}(\boldsymbol{\mu}), \mu_s) \mathbf{G}_{\mu_g}^{-T} : \nabla \mathbf{e}_N dx = \\ & = - \int_{\Omega_s} J_{\mu_g} K_{\mu_g} \sigma_f(\mathbf{u}_{f,N}^{i+1}(\boldsymbol{\mu}), p_{f,N}^{i+1,j+1}(\boldsymbol{\mu})) \mathbf{F}_{\mu_g}^{-T} \mathbf{G}_{\mu_g}^{-T} \mathbf{n}_f \cdot \mathbf{e}_N dx. \end{aligned}$$

5.4. Numerical results. We now present some numerical results for the test case with a geometrical and physical parametrization. The original configuration, the intermediate configuration and the reference configuration are the ones depicted in Figure 7. The geometrical constants of the problem are the same ones of the previous test case; indeed, the channel is 2.5cm high, and it is 10cm long; the leaflets length is represented by the geometrical parameter $\mu_g \in [0.8, 1.0]$, and the leaflets are situated 1cm downstream the inlet boundary (left vertical boundary of the channel), and they are 0.2cm thick. An affine mapping T is chosen, in order to deform the reference configuration $\hat{\Omega}$, obtained for $\mu_g = 1$ cm, into the intermediate configuration $\tilde{\Omega}(\boldsymbol{\mu})$. Top and bottom walls of the blue fluid domain are assumed to be rigid, thus both the displacement $\mathbf{d}_f(\boldsymbol{\mu})$ and the fluid velocity $\mathbf{u}_f(\boldsymbol{\mu})$ are set to zero. Homogeneous Neumann condition is imposed on $\mathbf{u}_f(\boldsymbol{\mu})$ on the outlet; a pressure profile $p_{in}(t)$ is described at the inlet, where:

$$p_{in}(t) = \begin{cases} 5 - 5 \cos\left(\frac{2\pi t}{T_{in}}\right) & \text{for } t \leq 0.1s \\ 5 & \text{for } t > 0.1s, \end{cases}$$

and $T_{in} = 0.4$ s. The tolerance chosen for the implicit step of the whole algorithm is $\varepsilon = 10^{-6}$.

For the simulation, we use a timestep $\Delta t = 10^{-4}$, for a maximum number of timesteps $N_T = 800$, thus $T = 0.08s$. Table 3 summarizes the details of the offline stage and of the FE discretization. Figure 11 shows three different examples of the behaviour of the leaflets, according to the change of the physical and/or of the geometrical parameters: all the pictures represent the online displacement of the solid at the final timestep of the simulation, namely for $t = 0.08s$. The results have been obtained using $N_d = 100$ reduced basis for the displacement; as we can see from Figure 11a and 11b, independently on the length of the leaflets, an increase in the shear modulus leads to a material that is much more hard to deform. On the contrary, for a fixed value of the properties of the material under consideration, and increase of the length of the leaflets leads to an increase in the displacement. As the results show, our reduced order model is able to capture small deformations of the solid, and it is also able to reproduce variations and changes in the behaviour of the leaflets, also at very small magnitudes.

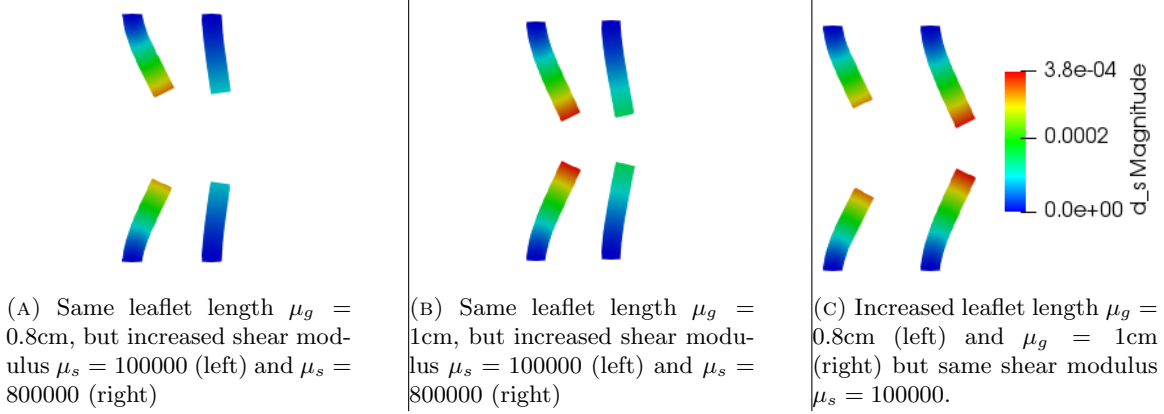


FIGURE 11. Reduced order solid displacement $\mathbf{d}_s^N(\boldsymbol{\mu})$. Comparison of different behaviours of the material, for different values of the geometrical and physical parameters. From left to right: same leaflets length (length of 0.8cm) and increased shear modulus ($\mu_s = 100000, 800000$); same leaflet length (length of 1cm) and increased shear modulus ($\mu_s = 100000, 800000$); increased leaflet length ($\mu_g = 0.8, 1.0$ cm), and same shear modulus $\mu_s = 100000$.

6. CONCLUSIONS

In this manuscript we presented the details of the implementation of a Reduced Order Model algorithm designed to address FSI problems, in the time dependent case, and possibly in the presence of a geometrical parametrization of the domain, and in the presence of a physical parametrization as well. We have designed a RBM that is based on a partitioned procedure: the main advantage of this is given by the fact that, by solving separately the fluid and the solid problem, we are not only able to lower the dimension of the systems to be solved in the online phase, but we also have a better control on the number of variables that are needed, avoiding, for example, to work with Lagrange multipliers to impose the coupling conditions, as would be instead the case if we used a monolithic approach. The reduced basis functions are generated through a Proper Orthogonal Decomposition on the set of snapshots, and the introduction of a change of variable in the fluid problem formulation allows, again, to avoid the use of Lagrange multipliers to impose non-homogeneous boundary conditions. The procedure that we have proposed aims at extending the work presented in [9] to the case of the coupling between an incompressible fluid and a thick, two dimensional structure, also in the presence of geometrical parametrization. The results that we have obtained confirm the following aspects:

- introducing a change of variable in fluid explicit step allows us to avoid the introduction of a further unknown in the system, namely a Lagrange multiplier, in order to impose non homogeneous boundary conditions at the fluid–structure interface;
- the choice of not performing a POD directly on the snapshots of the mesh displacement \mathbf{d}_f allows, again, to avoid the introduction of another Lagrange multiplier to impose the continuity of the displacement at the fluid–structure interface ($\mathbf{d}_f = \mathbf{d}_s$ on Γ_{FSI}). In addition to this, another advantage is represented by the choice of extending harmonically the solid displacement basis functions $\{\Phi\}_{i=1}^{N_d}$: indeed, this extension accounts for just a small additional offline cost, namely the solution of N_d harmonic problems;
- during the online phase, computing the reduced mesh displacement through the step (34) translates in *no additional online cost*: indeed the computation of the reduced mesh displacement does not require the solution of an harmonic problem, but requires instead a linear combination of the basis functions $\{\Phi_{d_f}^k\}_{i=1}^{N_d}$, with coefficients that were computed by the algorithm at the previous timestep. Moreover, the coupling condition that imposes

the continuity of the displacements at the fluid–structure interface is automatically satisfied, thanks to the way we have defined the reduced basis for \mathbf{d}_f .

In addition to the list of remarks presented, another very important detail of the procedure presented in this manuscript is the following: we did not employ a supremizer enrichment of the fluid velocity space, as it is the usual case for the RBM, in order to obtain a stable approximation of the fluid pressure in the online phase. Our choice is motivated by the fact that, even at the Finite Element level, the Chorin–Temam projection scheme with the pressure Poisson formulation can be applied successfully also to velocity–pressure FE spaces that do not satisfy the inf–sup condition, see [35]. This remark is very convenient also at the reduced order level, since it allows to obtain a stable approximation of the fluid pressure, without relying on the introduction of the supremizer unknown, thus limiting the dimension of the system to be solved online.

While testing this algorithm, we have seen that a partitioned procedure is demanding from the computational time point of view: this drawback is represented by the fact that, in the imposition of the coupling conditions through a Robin boundary condition, the constant α_{ROB} that makes the procedure more stable is heavily dependent on the timestep used. If we choose a timestep that is too big, the coupling becomes very weak and the algorithm becomes somehow insensitive to the effect of the interaction between the two physics. Aside from this aspect, which is peculiar to segregated approaches, the designed Reduced Basis Method performs very well, and thanks to the choice of a pressure Poisson formulation and to the derivation of the basis functions for the fluid displacement directly from the basis functions of the solid displacement, we have been able to limit the number of unknowns in the online stage.

It is also important to mention the fact that one can recover an efficient online–offline splitting thanks to the Empirical Interpolation Method (EIM), see for example [11, 45, 8]. The EIM has not been used in this work, as we wanted to focus on the development and test of a reduced order segregated procedure for FSI problems which involve the coupling of an incompressible fluid with an elastic structure; this can be seen as a natural future perspective for this work. Future perspectives also include the following aspects: the design of an alternative coupling of the fluid and solid problem, so that we can hopefully mitigate the strong dependence of the Robin constant α_{ROB} on the timestep used in the numerical simulations, and the integration of a Greedy algorithm within the design of the reduced basis. Indeed, even though for our test case the choice of uniform sampling in the parameter space \mathcal{P} was sufficient to obtain a good set of snapshots, this may not be the case for other problems; an alternative is represented by a Lagrangian sampling, but, again, this somehow relies on some kind of a priori knowledge of the physical phenomenon, whereas a Greedy procedure would just rely on the availability of an a posteriori error estimator.

ACKNOWLEDGMENTS

We acknowledge the support by European Union Funding for Research and Innovation – Horizon 2020 Program – in the framework of European Research Council Executive Agency: Consolidator Grant H2020 ERC CoG 2015 AROMA-CFD project 681447 “Advanced Reduced Order Methods with Applications in Computational Fluid Dynamics” (PI Prof. Gianluigi Rozza). We also acknowledge the INDAM-GNCS project “Tecniche Numeriche Avanzate per Applicazioni Industriali”. Nonino also acknowledges the support of the Austrian Science Fund (FWF) project F65 “Taming complexity in Partial Differential Systems” and the Austrian Science Fund (FWF) project P 33477. Numerical simulations have been obtained with the extension *multiphenics* of *FEniCS* [31, 42] for the high fidelity part, and RBniCS [57] for the reduced order part. We acknowledge developers and contributors of each of the aforementioned libraries.

APPENDIX

We propose here all the calculation that leads to the formulation of Robin boundary conditions for a projection–based semi–implicit coupling scheme. The final goal is to compute the constant α_{ROB} that improves the stability of the implicit coupling step, for a problem where we couple an incompressible fluid with a thick elastic structure. All the calculations presented here are inspired

by the work of [27, 10]. The goal here is to find suitable Robin conditions, in a situation where the structure is no longer considered to be one dimensional, and its behaviour is described by the linear elasticity equation. What follows is inspired by the idea proposed in [10].

We first begin with a simple test case: the deformation of the structure is so small, that we can consider the domain as being fixed. Let Ω_f be the fluid domain, Ω_s the solid domain, and Γ_{FSI} the fluid–structure interface.

The fluid problem reads as follows: for $t \in [0, T]$, find $\mathbf{u}_f(t): \Omega_f \mapsto \mathbb{R}^2$, $p(t): \Omega_f \mapsto \mathbb{R}$ and $\mathbf{d}_s(t): \Omega_s \mapsto \mathbb{R}^2$ such that

$$(35) \quad \begin{cases} \rho_f(\partial_t \mathbf{u}_f + (\mathbf{u}_f \cdot \nabla) \mathbf{u}_f) - \operatorname{div} \sigma_f(\mathbf{u}_f, p) = 0 & \text{in } \Omega_f, \\ \operatorname{div} \mathbf{u}_f = 0 & \text{in } \Omega_f, \\ \rho_s \partial_{tt} \mathbf{u}_s - \operatorname{div} P(\mathbf{d}_s) = 0 & \text{in } \Omega_s, \end{cases}$$

where $P(\mathbf{d}_s)$ is defined as

$$P(\mathbf{d}_s) = \lambda_s (\nabla \cdot \mathbf{d}_s) \mathbf{I} + \mu_s \varepsilon(\mathbf{d}_s), \quad \varepsilon(\mathbf{d}_s) = (\nabla \mathbf{d}_s + \nabla^T \mathbf{d}_s).$$

Here \mathbf{I} is the 2×2 identity matrix, and λ_s, μ_s are the Lamé coefficients of the solid.

The coupling conditions are:

$$\begin{cases} \mathbf{u}_f = \partial_t \mathbf{d}_s, & \text{on } \Gamma_{FSI}, \\ \sigma_f(\mathbf{u}_f, p) \mathbf{n}_f = P(\mathbf{d}_s) \mathbf{n}_f, & \text{on } \Gamma_{FSI}. \end{cases}$$

The key ingredient is the observation that the solid problem (35)₃ is an hyperbolic PDE, that has two wave velocities:

$$c_p = \sqrt{\frac{\lambda_s + 2\mu_s}{\rho_s}} \quad c_s = \sqrt{\frac{\mu_s}{\rho_s}}$$

If one writes equation (35)₃ in the normal component with respect to Γ_{FSI} , then it is possible to compute the characteristics of the corresponding wave equation, and the characteristic variables. These are the characteristic variables that are *outgoing*, i.e. that are transferred from the solid to the fluid:

$$\mathcal{B}(P, \partial_t \mathbf{d}_s) = P(\mathbf{d}_s) \mathbf{n}_f \cdot \mathbf{n}_f + z_p \partial_t \mathbf{d}_s \cdot \mathbf{n}_f, \quad \mathcal{B}_\tau(P, \partial_t \mathbf{d}_s) = P(\mathbf{d}_s) \mathbf{n}_f \cdot \boldsymbol{\tau} + z_s \partial_t \mathbf{d}_s \cdot \boldsymbol{\tau},$$

whereas the characteristic variables that are *incoming* to the solid are:

$$\mathcal{A}(P, \partial_t \mathbf{d}_s) = P(\mathbf{d}_s) \mathbf{n}_f \cdot \mathbf{n}_f - z_p \partial_t \mathbf{d}_s \cdot \mathbf{n}_f, \quad \mathcal{A}_\tau(P, \partial_t \mathbf{d}_s) = P(\mathbf{d}_s) \mathbf{n}_f \cdot \boldsymbol{\tau} - z_s \partial_t \mathbf{d}_s \cdot \boldsymbol{\tau},$$

where $z_p = \rho_s c_p$ and $z_s = \rho_s c_s$ are the solid impedances, while \mathbf{n}_f and $\boldsymbol{\tau}$ are, respectively, the unit normal to Γ_{FSI} pointing outward the fluid domain, and $\boldsymbol{\tau}$ is the tangential unit vector to Γ_{FSI} . The key point, therefore, is to impose the balance of these informations at the interface Γ_{FSI} :

$$(36) \quad \mathcal{B}(\sigma_f^f, \mathbf{u}_f) = \mathcal{B}(P(\mathbf{d}_s), \partial_t \mathbf{d}_s), \quad \mathcal{B}_\tau(\sigma_f^f, \mathbf{u}_f) = \mathcal{B}_\tau(P(\mathbf{d}_s), \partial_t \mathbf{d}_s)$$

and

$$(37) \quad \mathcal{A}(\sigma_f^f, \mathbf{u}_f) = \mathcal{A}(P(\mathbf{d}_s), \partial_t \mathbf{d}_s), \quad \mathcal{A}_\tau(\sigma_f^f, \mathbf{u}_f) = \mathcal{A}_\tau(P(\mathbf{d}_s), \partial_t \mathbf{d}_s).$$

From equation (36) it follows in particular that:

$$(38) \quad P(\mathbf{d}_s) \mathbf{n}_f \cdot \mathbf{n}_f + z_p \partial_t \mathbf{d}_s \cdot \mathbf{n}_f = \sigma_f^f(\mathbf{u}_f, p) \mathbf{n}_f \cdot \mathbf{n}_f + z_p \mathbf{u}_f \cdot \mathbf{n}_f,$$

and keeping the structure of the semi-implicit coupling scheme in mind, we can re-write the discretized in time version of the previous equation as follows:

$$(39) \quad \lambda_s \operatorname{tr} \varepsilon(\mathbf{d}_s^{i+1, \star}) + \mu_s \varepsilon(\mathbf{d}_s^{i+1, \star}) \mathbf{n}_f \cdot \mathbf{n}_f + z_p D_t \mathbf{d}_s^{i+1, \star} \cdot \mathbf{n}_f = -p^{i+1} + \mu_f \varepsilon(\tilde{\mathbf{u}}_f^{i+1}) \mathbf{n}_f \cdot \mathbf{n}_f + z_p \mathbf{u}_f^{i+1} \cdot \mathbf{n}_f.$$

Now let us remember that we choose to impose strongly the coupling condition:

$$\sigma_f(\tilde{\mathbf{u}}_f^{i+1}, p^{i+1}) \mathbf{n}_f = P(\mathbf{d}_s^{i+1}) \mathbf{n}_f \quad \text{on } \Gamma_{FSI},$$

so it follows that:

$$\sigma_f(\tilde{\mathbf{u}}_f^{i+1}, p^{i+1, \star}) \mathbf{n}_f = P(\mathbf{d}_s^{i+1, \star}) \mathbf{n}_f \quad \text{on } \Gamma_{FSI},$$

and so we have the following equation, obtained projecting the previous coupling condition along \mathbf{n}_f :

$$-p^{i+1,*} + \mu_f \varepsilon(\tilde{\mathbf{u}}_f^{i+1}) \mathbf{n}_f \cdot \mathbf{n}_f = \lambda_s \text{tr} \varepsilon(\mathbf{d}^{i+1,*}) + \mu_s \varepsilon(\mathbf{d}_s^{i+1,*}) \mathbf{n}_f \cdot \mathbf{n}_f.$$

Now, according to the structure of our partitioned algorithm, it follows, by substituting the previous equation into equation (39), that:

$$-p^{i+1} + z_p \mathbf{u}_f^{i+1} \cdot \mathbf{n}_f = -p^{i+1,*} + z_p D_t \mathbf{d}_s^{i+1,*} \cdot \mathbf{n}_f.$$

Again, if we adopt a pressure Poisson formulation in our algorithm, then we substitute $\mathbf{u}_f^{i+1} = \tilde{\mathbf{u}}_f^{i+1} - \frac{\Delta t}{\rho_f} \nabla p^{i+1}$, and we arrive to the final expression of the Robin coupling condition:

$$(40) \quad -\alpha_{rob} p^{i+1} - \nabla p^{i+1} \cdot \mathbf{n}_f = -\alpha_{rob} p^{i+1,*} + \rho_f D_{tt} \mathbf{d}_s^{i+1,*} \cdot \mathbf{n}_f.$$

Thus the expression of the Robin coupling conditions remains unchanged, the only thing that changes is the Robin constant α_{rob} , which now is $\alpha_{rob} = \frac{\rho_f}{z_p \Delta t}$: the coupling constant now depends also on the timestep, unlike in the case of a thin structure. Therefore if we choose a timestep that is too big, α_{rob} goes to zero and thus the algorithm becomes insensitive to the effects of the interaction between fluid and structure.

6.1. Coupling of an incompressible fluid in ALE formulation with a thick walled structure. The final step of these calculations is to formulate the proper Robin boundary conditions in the situation where we are incorporating an Arbitrary Lagrangian Eulerian formulation to the problem description.

Let us call $\Omega_f(t)$ the fluid domain at time t , and let $\hat{\Omega}_f$ be a reference configuration. Let $\mathcal{A}_f(t): \hat{\Omega}_f \mapsto \Omega_f(t)$ be the ALE map that maps the reference configuration to the actual physical domain. Let \mathbf{F} be the jacobian of \mathcal{A}_f and let J be its determinant. Let \mathbf{u}_f, p be the fluid velocity and the fluid pressure, defined on the physical domain $\Omega_f(t)$, and let $\hat{\mathbf{u}}_f$ and \hat{p} be their counterparts in the reference configuration, let $\hat{\Omega}_s$ be the solid reference domain (which coincides with the Lagrangian domain for the solid), and let $\hat{\Gamma}_{FSI}$ be the FSI interface in the reference configuration.

In order to obtain the Robin coupling condition in the ALE framework, it is sufficient to perform a pull-back of the equation (40) on the reference configuration, keeping in mind that the pull-back of the normal \mathbf{n}_f to the fluid–structure interface in the original configuration is given by $J\mathbf{F}^{-T}\hat{\mathbf{n}}_f$. With this remark in mind, we obtain the following Robin coupling condition in the ALE setting:

$$-\frac{\rho_f}{z_p \Delta t} \hat{p}^{i+1} - \mathbf{F}^{-T} \hat{\nabla} \hat{p}^{i+1} \cdot J\mathbf{F}^{-T} \hat{\mathbf{n}}_f = -\frac{\rho_f}{z_p \Delta t} \hat{p}^{i+1,*} + \rho_f D_{tt} \hat{\mathbf{d}}_s^{i+1,*} \cdot J\mathbf{F}^{-T} \hat{\mathbf{n}}_f.$$

REFERENCES

- [1] D. Amsallem, J. Cortial, and C. Farhat. Toward real-time computational-fluid-dynamics-based aeroelastic computations using a database of reduced-order information. *Aiaa Journal - AIAA J*, 48:2029–2037, 2010.
- [2] M. Astorino, F. Chouly, and M. A. Fernández. Robin based semi-implicit coupling in Fluid–Structure Interaction: stability analysis and numerics. *SIAM Journal on Scientific Computing*, 31(6):4041–4065, 2010.
- [3] S. Badia, F. Nobile, and C. Vergara. Fluid–structure partitioned procedures based on Robin transmission conditions. *Journal of Computational Physics*, 227(14):7027 – 7051, 2008.
- [4] S. Badia, A. Quaini, and A. Quarteroni. Splitting methods based on algebraic factorization for Fluid–Structure Interaction. *SIAM Journal on Scientific Computing*, 30(4):1778–1805, 2008.
- [5] S. Badia, A. Quaini, and A. Quarteroni. Coupling Biot and Navier–Stokes equations for modelling fluid–poroelastic media interaction. *Journal of Computational Physics*, 228(21):7986 – 8014, 2009.
- [6] F. Ballarin, E. Faggiano, S. Ippolito, Manzoni, A. Quarteroni, G. Rozza, and R. Scrofani. Fast simulations of patient-specific haemodynamics of coronary artery bypass grafts based on a POD–Galerkin method and a vascular shape parametrization. *Journal of Computational Physics*, 315:609–628, 2016.
- [7] F. Ballarin, A. Manzoni, A. Quarteroni, and G. Rozza. Supremizer stabilization of POD–Galerkin approximation of parametrized steady incompressible Navier–Stokes equations. *International Journal for Numerical Methods in Engineering*, 102(5):1136–1161, 2015.
- [8] F. Ballarin and G. Rozza. POD–Galerkin monolithic reduced order models for parametrized Fluid–Structure Interaction problems. *International Journal for Numerical Methods in Fluids*, 82(12):1010–1034, 2016.

- [9] F. Ballarin, G. Rozza, and Y. Maday. Reduced-order semi-implicit schemes for Fluid–Structure Interaction problems. In *Model Reduction of Parametrized Systems*, volume 17 of *MS&A series*, pages 149–167. Springer, Cham, 2017.
- [10] J. W. Banks, W. D. Henshaw, and D. W. Schwendeman. An analysis of a new stable partitioned algorithm for FSI problems. Part I: incompressible flow and elastic solids. *Journal of Computational Physics*, 269:108 – 137, 2014.
- [11] M. Barrault, Y. Maday, N. C. Nguyen, and A. T. Patera. An Empirical Interpolation Method: application to efficient reduced-basis discretization of partial differential equations. *Comptes Rendus Mathématique*, 339(9):667–672, 2004.
- [12] S. Basting, A. Quaini, R. Glowinski, and S. Čanić. On the implementation and benchmarking of an extended ALE Method for FSI problems. In *Fluid-Structure Interaction: Modeling, Adaptive Discretizations and Solvers*, pages 3–39. 2017.
- [13] L. Bertagna and A. Veneziani. A model reduction approach for the variational estimation of vascular compliance by solving an inverse Fluid–Structure Interaction problem. *Inverse Problems*, 30(5):055006, 2014.
- [14] T. Bui-Thanh, M. Damodaran, and K. Willcox. Proper orthogonal decomposition extensions for parametric applications in compressible aerodynamics. In *21st AIAA Applied Aerodynamics Conference, Orlando, Florida*, 2003.
- [15] K. Carlberg, C. Farhat, J. Cortial, and D. Amsallem. The GNAT method for nonlinear model reduction: Effective implementation and application to computational fluid dynamics and turbulent flows. *Journal of Computational Physics*, 242:623 – 647, 2013.
- [16] P. Causin, J. F. Gerbeau, and F. Nobile. Added-mass effect in the design of partitioned algorithms for fluid–structure problems. *Computer Methods in Applied Mechanics and Engineering*, 194(42):4506 – 4527, 2005.
- [17] A. Cesmelioglu, H. Lee, A. Quaini, K. Wang, and S. Y. Yi. Optimization-Based Decoupling Algorithms for a Fluid-Poroelastic System. In *Topics in Numerical Partial Differential Equations and Scientific Computing*, pages 79–98. Springer, New York, NY, 2016.
- [18] E. A. Christensen., M. Brøns, and J. N. Sørensen. Evaluation of Proper Orthogonal Decomposition–based decomposition techniques applied to parameter-dependent nonturbulent flows. *SIAM Journal on Scientific Computing*, 21(4):1419–1434, 1999.
- [19] C. M. Colciago and S. Deparis. Reduced Numerical Approximation for Fluid–Structure Interaction problems with applications in haemodynamics. *Frontiers in Applied Mathematics and Statistics*, 4, 2018.
- [20] S. Deparis, D. Forti, G. Grandperrin, and A. Quarteroni. FaCSI: A block parallel preconditioner for fluid–structure interaction in hemodynamics. *Journal of Computational Physics*, 327:700–718, 2016.
- [21] A. Derkevorkian, P. Avery, C. Farhat, J. Rabinovitch, and L. Peterson. Effects of structural parameters on the FSI simulation of supersonic parachute deployments. In *AIAA Aviation 2019 Forum, Dallas, Texas*.
- [22] J. Donea, S. Giuliani, and J. P. Halleux. An Arbitrary Lagrangian–Eulerian finite element method for transient dynamic Fluid–Structure Interactions. *Computer Methods in Applied Mechanics and Engineering*, 33(1):689 – 723, 1982.
- [23] D. Errate, M. J. Esteban, and Y. Maday. Couplage fluid–structure. Un modele simplifié en dimension 1. *Comptes rendus de l’Académie des sciences. Série 1, Mathématique*, 318:275–281, 1994.
- [24] C. Farhat and V. K. Lakshminarayan. An ALE formulation of embedded boundary methods for tracking boundary layers in turbulent Fluid–Structure Interaction problems. *Journal of Computational Physics*, 263:53 – 70, 2014.
- [25] M. A. Fernández. Incremental displacement-correction schemes for incompressible Fluid–Structure Interaction. *Numerische Mathematik*, 123:21 – 65, 2013.
- [26] M. A. Fernández, J. F. Gerbeau, and C. Grandmont. A projection semi-implicit scheme for the coupling of an elastic structure with an incompressible fluid. *International Journal for Numerical Methods in Engineering*, 69(4):794–821, 2007.
- [27] M. A. Fernández, M. Landajuela, and M. Vidrascu. Fully decoupled time-marching schemes for incompressible fluid/thin-walled structure interaction. *Journal of Computational Physics*, 297:156 – 181, 2015.
- [28] M. A. Fernández, J. Mullaert, and M. Vidrascu. Explicit Robin–Neumann schemes for the coupling of incompressible fluids with thin-walled structures. *Computer Methods in Applied Mechanics and Engineering*, 267:566 – 593, 2013.
- [29] D. Forti, M. Bukac, A. Quaini, S. Canic, and S. Deparis. A Monolithic Approach to Fluid–Composite Structure Interaction. *Journal of Scientific Computing*, 72(1):396–421, 2017.
- [30] M. W. Gee, U. Küttler, and W. A. Wall. Truly monolithic algebraic multigrid for fluid–structure interaction. *International Journal for Numerical Methods in Engineering*, 85(8):987–1016, 2011.
- [31] multiphenics - easy prototyping of multiphysics problems in FEniCS. <http://mathlab.sissa.it/multiphenics>, 2016.
- [32] C. Grandmont, V. Guimet, and Y. Maday. Numerical analysis of some decoupling techniques for the approximation of the unsteady Fluid–Structure Interaction. *Mathematical Models and Methods in Applied Sciences*, 11(08):1349–1377, 2001.
- [33] C. Grandmont and Y. Maday. Existence de solutions d’un problème de couplage fluide-structure bidimensionnel instationnaire. *Comptes Rendus de l’Académie des Sciences - Series I - Mathematics*, 326(4):525 – 530, 1998.
- [34] J. L. Guermond and L. Quartapelle. Calculation of incompressible viscous flows by an unconditionally stable projection fem. *Journal of Computational Physics*, 132(1):12 – 33, 1997.

- [35] J. L. Guermond and L. Quartapelle. On stability and convergence of projection methods based on pressure poisson equation. *International Journal for Numerical Methods in Fluids*, 26(9):1039–1053, 1998.
- [36] J. L. Guermond and L. Quartapelle. On the approximation of the unsteady navier–stokes equations by finite element projection methods. *Numerische Mathematik*, 80:207–238, 1998.
- [37] M. E. Gurtin. *An Introduction to Continuum Mechanics*. Mathematics in Science and Engineering. Elsevier Science, Amsterdam, 1982.
- [38] T. Hughes, W. Liu, and T. Zimmermann. Lagrangian–Eulerian finite element formulation for incompressible viscous flows. *Computer Methods in Applied Mechanics and Engineering*, 29(3):329–349, 1981.
- [39] T. Lassila, A. Manzoni, A. Quarteroni, and G. Rozza. Model order reduction in fluid dynamics: challenges and perspectives. In *Reduced Order Methods for Modeling and Computational Reduction*, volume 9 of *MS&A series*, pages 235–273. Springer, Cham, 2014.
- [40] T. Lassila, A. Quarteroni, and G. Rozza. A reduced basis model with parametric coupling for Fluid–Structure Interaction problems. *SIAM Journal on Scientific Computing*, 34(2):1187–1213, 2012.
- [41] T. Lieu, C. Farhat, and M. Lesoinne. Reduced-order fluid/structure modeling of a complete aircraft configuration. *Computer Methods in Applied Mechanics and Engineering*, 195(41):5730 – 5742, 2006.
- [42] A. Logg, K. Mardal, and G. Wells. *Automated Solution of Differential Equations by the Finite Element Method*. Springer-Verlag, Berlin, 2012.
- [43] M. Lombardi, N. Parolini, A. Quarteroni, and G. Rozza. Numerical simulation of sailing boats: dynamics, FSI, and shape optimization. In *Variational Analysis and Aerospace Engineering: Mathematical Challenges for Aerospace Design*, volume 66 of *Springer Optimization and its Applications*, pages 339–377, Boston, MA, 2012. Springer.
- [44] Y. Maday. Analysis of coupled models for fluid-structure interaction of internal flows. In *Cardiovascular Mathematics: Modeling and simulation of the circulatory system*, pages 279–306. Springer, Milan, 2009.
- [45] Y. Maday, O. Mula, A. T. Patera, and M. Yano. The generalized empirical interpolation method: stability theory on Hilbert spaces with an application to the stokes equation. *Computer Methods in Applied Mechanics and Engineering*, 287:310–334, 2015.
- [46] M. Nonino, F. Ballarin, and G. Rozza. A monolithic and a partitioned reduced basis method for fluid–structure interaction problems. *Fluids*, 6(6), 2021.
- [47] M. Nonino, F. Ballarin, G. Rozza, and Y. Maday. Overcoming slowly decaying Kolmogorov n-width by transport maps: application to model order reduction of fluid dynamics and Fluid–Structure Interaction problems. arXiv:1911.06598, 2019.
- [48] A. Quaini. *Algorithms for Fluid–Structure Interaction problems arising in hemodynamics*. PhD thesis, EPFL, Lausanne, 2009.
- [49] A. Quarteroni and L. Formaggia. Mathematical modelling and numerical simulation of the cardiovascular system. *Handbook of Numerical Analysis*, 12:3–127, 2004.
- [50] A. Quarteroni, G. Rozza, and A. Manzoni. Certified reduced basis approximation for parametrized partial differential equations and applications. *Journal of Mathematics in Industry*, 1, 2011.
- [51] A. Quarteroni, M. Tuveri, and A. Veneziani. Computational vascular fluid dynamics: problems, models and methods. *Computing and Visualization in Science*, 2:163–197, 2000.
- [52] J. Rabinovitch, D. Z. Huang, R. Borker, P. Avery, C. Farhat, A. Derkevorkian, and L. Peterson. Towards a validated fsi computational framework for supersonic parachute deployments. In *AIAA Aviation 2019 Forum*.
- [53] T. Richter. *Fluid–structure Interactions. Model, Analysis and Finite Element*, volume 118 of *Lecture Notes in Computational Science and Engineering*. Springer, Cham, 2017.
- [54] G. Rozza, D. B. P. Huynh, and A. Manzoni. Reduced basis approximation and a posteriori error estimation for Stokes flows in parametrized geometries: Roles of the inf-sup stability constants. *Numerische Mathematik*, 125(1):115–152, 2013.
- [55] G. Rozza, D. B. P. Huynh, and A. T. Patera. Reduced basis approximation and a posteriori error estimation for affinely parametrized elliptic coercive partial differential equations: Application to transport and continuum mechanics. *Archives of Computational Methods in Engineering*, 15(3):229–275, 2008.
- [56] G. Rozza and K. Veroy. On the stability of the reduced basis method for Stokes equations in parametrized domains. *Computer Methods in Applied Mechanics and Engineering*, 196(7):1244–1260, 2007.
- [57] RBniCS - reduced order modelling in FEniCS. <http://mathlab.sissa.it/rbnics>, 2015.
- [58] Y. Wang, A. Quaini, S. Čanić, M. Vukicevic, and S. H. Little. 3d experimental and computational analysis of eccentric mitral regurgitant jets in a mock imaging heart chamber. *Cardiovascular Engineering and Technology*, 8(4):419–438, 2017.
- [59] Y. Wu and X. C. Cai. A fully implicit domain decomposition based ALE framework for three-dimensional Fluid–Structure Interaction with application in blood flow computation. *Journal of Computational Physics*, 258:524 – 537, 2014.